ACS Biomaterials SCIENCE & ENGINEERING

pubs.acs.org/journal/abseba

Review

Integration of MXene and Microfluidics: A Perspective

Moein Safarkhani, Bahareh Farasati Far, Eder C. Lima, Shima Jafarzadeh, Pooyan Makvandi, Rajender S. Varma, YunSuk Huh,* Majid Ebrahimi Warkiani,* and Navid Rabiee*

Cite This: *ACS Biomater. Sci. Eng.* 2024, 10, 657−676

Read Online

ACCESS | Metrics & More | Article Recommendations

ABSTRACT: The fusion of MXene-based materials with microfluidics not only presents a dynamic and promising avenue for innovation but also opens up new possibilities across various scientific and technological domains. This Perspective delves into the intricate synergy between MXenes and microfluidics, underscoring their collective potential in material science, sensing, energy storage, and biomedical research. This intersection of disciplines anticipates future advancements in MXene synthesis and functionalization as well as progress in advanced sensing technologies, energy storage solutions, environmental applications, and biomedical breakthroughs. Crucially, the manufacturing and commercialization of MXene-based microfluidic devices, coupled with interdisciplinary collaborations, stand as pivotal considerations. Envisioning a future where MXenes and microfluidics collaboratively shape our technological landscape, addressing intricate challenges and propelling innovation forward necessitates a thoughtful approach. This viewpoint provides a comprehensive assessment of the current state of the field while outlining future prospects for the integration of MXene-based entities and microfluidics.

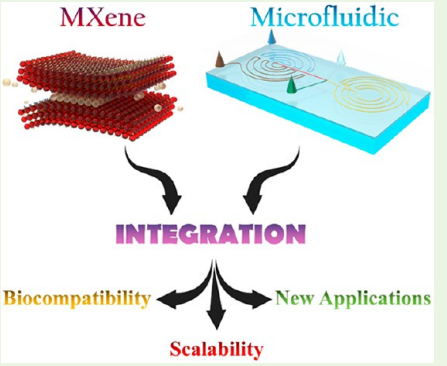

KEYWORDS: *MXene, microfluidics, biomedical engineering, sensor, wearables*

1. INTRODUCTION

Microfluidics entails the manipulation of fluids within extremely small channels, typically on a micrometer scale.[1] Over the past three decades, the promise of "lab-on-a-chip" microfluidic technologies has become increasingly evident.[2−5] This technology capitalizes on advantages like minimal consumption of samples and reagents, quick analysis facilitated by limited diffusion distances, coupled with the capacity to execute numerous analytical procedures within a compact device, resulting in efficient sample-to-answer processes.[6] Microfluidics serves as the foundational technology behind the creation of various point-of-care devices, which have played a pivotal role in advancing 3recisionn healthcare.[7,8] Currently, the focus is on developing systems that are straightforward to operate and manufacture and are readily accessible to end-users. An alternative approach to complex all-in-one micro-electromechanical systems (MEMS) entails the integration of uncomplicated microfluidic flow cells with an independent sensor unit. This strategy is favored due to potential manufacturing complexities associated with integrated MEMS devices.[9,10] In the realm of microfluidic electroanalytical sensors, a common practice involves microfluidic flow-cell technology construction based on either custom-developed or commercially available connecting electrodes. The advantage lies in the ability to replace the electrode, as surfaces can become fouled after repeated usage. Another popular micro-fluidic setup is the microfluidic paper-based analytical device (μPAD) that operates on capillary action, thus eliminating the need for pumps. Techniques such as screen printing, laser printing, and wax printing, are commonly employed techniques for crafting paper-based microfluidic devices[11−13] which are lightweight, easily manufacturable, and designed for single-use purposes. Notably, a variety of lateral flow-based fluidic devices have been successfully brought to market, including pregnancy tests and, more recently, home diagnostic kits for COVID-19. In the realm of electrochemical μPADs, paper-based electrodes are utilized as a key component.[14,15]

In the domain of chemical and biosensors, the central component that holds significance is the transducer, as it assumes a pivotal role in converting reaction or binding events into quantifiable signals. Within the field of biosensors, the occurrence of molecular recognition-mediated binding events on the sensor's surface has been conventionally transmuted into either chemical or light-based signal.[16−18] Nanomaterials, due to their inherent characteristics, have been effectual in generating signals that have found appliances in the advance-

Received: September 19, 2023
Revised: December 4, 2023
Accepted: December 5, 2023
Published: January 19, 2024

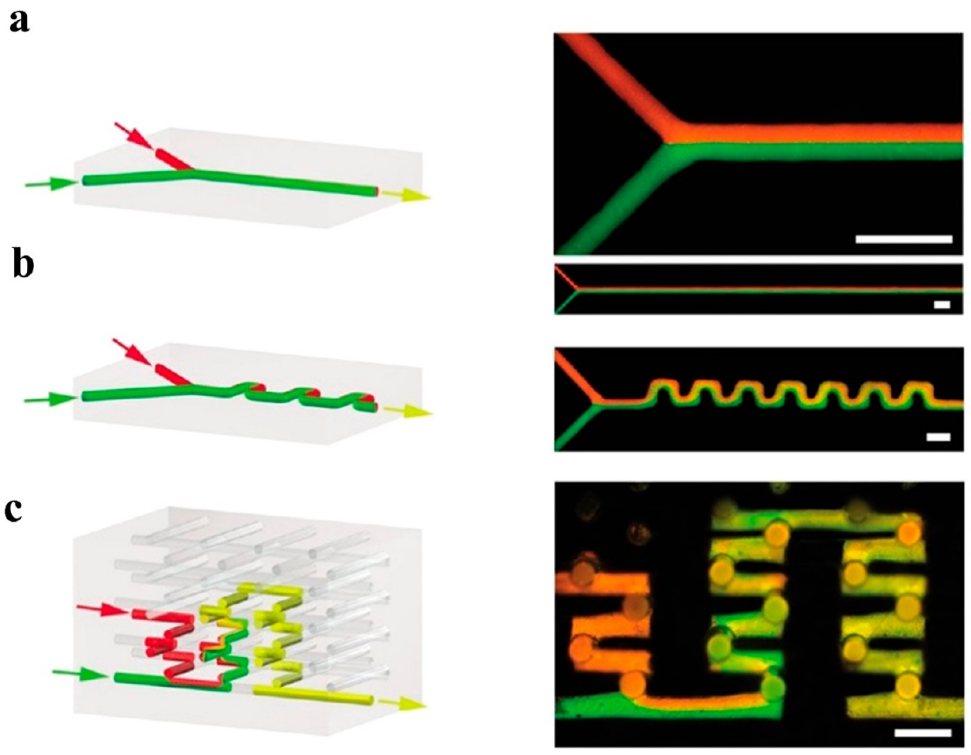

Figure 1. (a) Straight microchannel measuring 17 mm in length. (b) A square-wave microchannel with a length of 15 mm along the streamwise direction, featuring seven C-turns. (c) In the 3D setup, inside a spiral tower, the two fluids are injected at various intervals and subsequently mixed inside of two towers that are joined together. In all cases, the scale bars in the fluorescent microscope images are set at 0.5 mm for reference. Reproduced with permission from ref 32. Copyright 2003 Springer Nature.

ment of biosensors and chemo-sensors catering to healthcare and food safety sectors.[19−21] The utilization of these nanomaterials has been instrumental in the development of transducer systems. Nanomaterials are precisely defined by their dimensions, typically falling within the range of 1 to 100 nm or exhibiting at least one dimension within this nanoscale range. They are frequently classified into various dimensional configurations, encompassing 0D (particles), 1D (rods), 2D (sheets), and considerably extra convoluted 3D structures.[22−24] Notably, nanomaterials, namely, silver and gold nanoparticles, have gained widespread acceptance in the advancement of transducer technologies, especially in the domain of microfluidic biosensors. A noteworthy advantage lies in their remarkable surface area-to-volume ratio., which translates to a greater number of binding sites and more robust signals.[25−27] Additionally, many nanomaterials exhibit significant electrochemical activity, further contributing to robust signal generation. Moreover, these materials are relatively straightforward to synthesize, often display low toxicity (aligned with the Green Biomaterials principles), and can be conveniently adapted for diverse applications. The key attribute of nanomaterials lies in their fine-tuning of optical characteristics, which is possible thanks to the exceptional level of control that can be applied over particle size. In the field of microfluidic biosensors, optical techniques such as absorbance and fluorescence find extensive application as the most commonly employed methods for signal detection and measurement.[28−30] Various microfluidic systems for the synthesis of nanoparticles (including MXenes) can be classified into three distinct categories:[31] (i) mixing-oriented microfluidic reactors that rely on continuous flow for hydrodynamic mixing, (ii) multifield-driven microfluidic reactors, which combine hydrodynamic flow with various physical fields, and (iii) droplet-centered microfluidic reactors, which deploy segmented droplets as enclosed reacting chambers. Also, the critical process of nanoparticle fabrication involves mixing, wherein the generation of nanoparticles is initiated through solvent exchange. The size and monodispersity of nanoparticles are closely linked to the mixing time (τ_{mix}). When the duration of mixing is less than the nucleation time of nanoparticles ($\tau_{mix} < \tau_{agg}$), it leads to the production of small nanoparticles with excellent uniformity.

In contrast, when the mixing duration exceeds the nucleation period ($\tau_{mix} > \tau_{agg}$), it culminates in the creation of larger nanoparticles, characterized by wider size distributions. Within the microfluidic context, there is a prevailing presence of laminar flow attributes, which is evident through the observation of a low Reynolds number ($Re = \rho U D_h/\eta$). Here, ρ signifies fluid density; U denotes fluid velocity, D_h represents the cross-sectional dimension of the microchannel, and η indicates dynamic viscosity. This fluid flow consistently remains below the critical threshold, typically $\sim 10^3$, required to initiate turbulence. Within the confined microscale domains, effective mass transfer processes enable microfluidic systems to achieve impressively brief mixing durations, often on the order of 1×10^{-4} seconds. This remarkable acceleration translates to mixing rates up to 1000 times faster compared to their macroscopic counterparts. To optimize the mixing process under laminar conditions, a variety of methods have been devised for microscale applications at low to moderate Reynolds numbers. These methodologies can be categorized into three distinct approaches: 1D streamline-based, 2D, and 3D vortex-based mixing techniques as depicted in Figure 1a−c.[32]

https://doi.org/10.1021/acsbiomaterials.3c01361
ACS Biomater. Sci. Eng. 2024, 10, 657−676

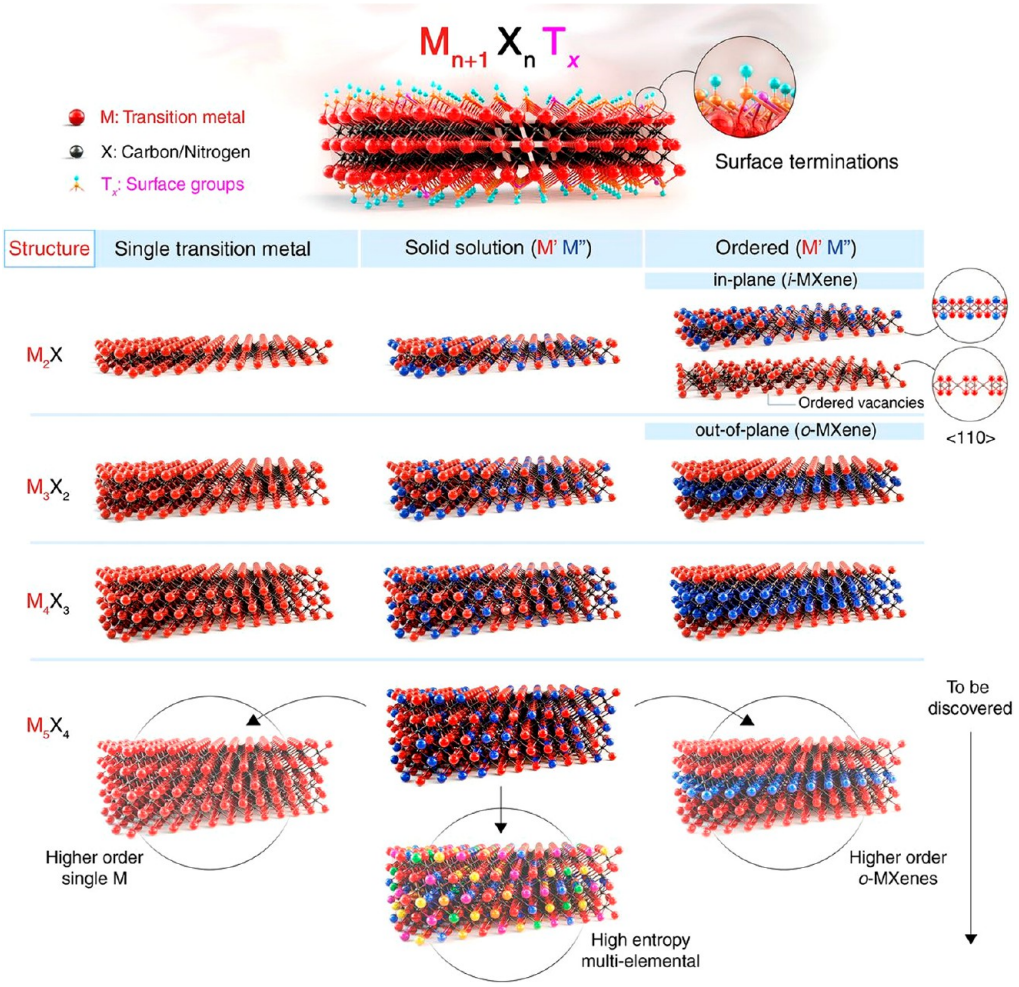

Figure 2. Schematic diagram of the structural configurations found in MXenes. These two-dimensional materials are characterized by a common chemical formula, $M_{n+1}X_nT_x$, where M stands for a member of transition metals, X for nitrogen and/or carbon, and Tx for terminations at the metal's surface. Depending on how many layers of transition metal (and carbon and/or nitrogen) are present in the MXene structure, *n* can take on values between 1 and 4. For example, specific instances include Ti_2CT_x (n = 1), $Ti_3C_2T_x$ (n = 2), $Nb_4C_3T_x$ (n = 3), and $(Mo,V)_5C_4T_x$ (n = 4). Recent research has uncovered $Mo_4VC_4T_x$, a solid solution MXene with five M layers that exhibit twinning within these M layers, representing a departure from previously known MXene structures.[44] Solid solutions or ordered arrangements can be formed from MXenes when one or more transition metal atoms occupy the M sites. These ordered structures encompass various types, including in-plane ordered varieties, referred to as i-MXenes (e.g., $(Mo_{2/3}Y_{1/3})_2CT_x$), in-plane vacancy structures (e.g., $W_{2/3}CT_x$), and out-of-plane ordered structures, known as o-MXenes. Two distinct configurations are possible in *o*-MXenes: one in which a single layer of M″ transition metal is sandwiched between two layers of M' transition metal (such as Mo_2TiC_2Tx), and the other in which two layers of M″ transition metals are also sandwiched between two layers of M' transition metal (e.g., $Mo_2Ti_2C_3T_x$). Additional configurations, namely the M_5X_4 structure's (bottom row) existence of one or three M″ layers sandwiched between M' layers, are still being considered. MXenes with high entropy and other higher-order single Mor o-MXenes are just two examples of the unproven possible structures represented in the diagram. Reproduced with permission from ref 45. Copyright 2021 Science.

Ever since the breakthrough of graphene, the spotlight has been firmly fixed on 2D nanomaterials due to their distinctive attributes compared with other types of nanomaterial. These 2D nanomaterials exhibit a unique structure where atomic layers are stacked, akin to the pages of a book, linked by weak Van der Waals forces. Numerous comprehensive articles underline the synthesis, manufacturing techniques, and properties of these 2D nanomaterials.[33−35] These materials can be broadly categorized into four principal groups: (i) MXenes, (ii) 2D metal oxides, (iii) the graphene family, and (iv) transition metal dichalcogenides (TMD). The graphene family extends its scope beyond nanostructures based solely on graphene, encompassing analogous materials such as graphitic carbon nitride ($g\text{-}C_3N_4$), hexagonal boron nitride, white graphene, black phosphorus, and various other related compounds. TMD compounds, characterized by the bonding of a metal element with two chalcogens (referred to as MX_2), are exemplified by materials like WS_2 and MoS_2 with a planar structure. The more recent additions to the 2D nanomaterials are MXenes, which contain a layer of carbon or nitrogen in between layers of a transition metal.[36−38] Further, zinc oxide and cerium oxide are examples of oxygen atoms linked to a metal nucleus that represent 2D metal oxides. The inherent properties of these 2D nanomaterials are striking: an elevated surface area resulting from their sheetlike structure, notable conductivity due to localized electronic states enabling charge carrier recombination, commendable optical characteristics, substantial mechanical strength, and considerable flexibility. This last trait holds significant importance for the advancement of flexible electronics, including wearable sensors[39−41] which may have a noticeable impact on healthcare.[42,43] In this Perspective, the discussion herein focuses on recent

https://doi.org/10.1021/acsbiomaterials.3c01361
ACS Biomater. Sci. Eng. 2024, 10, 657−676

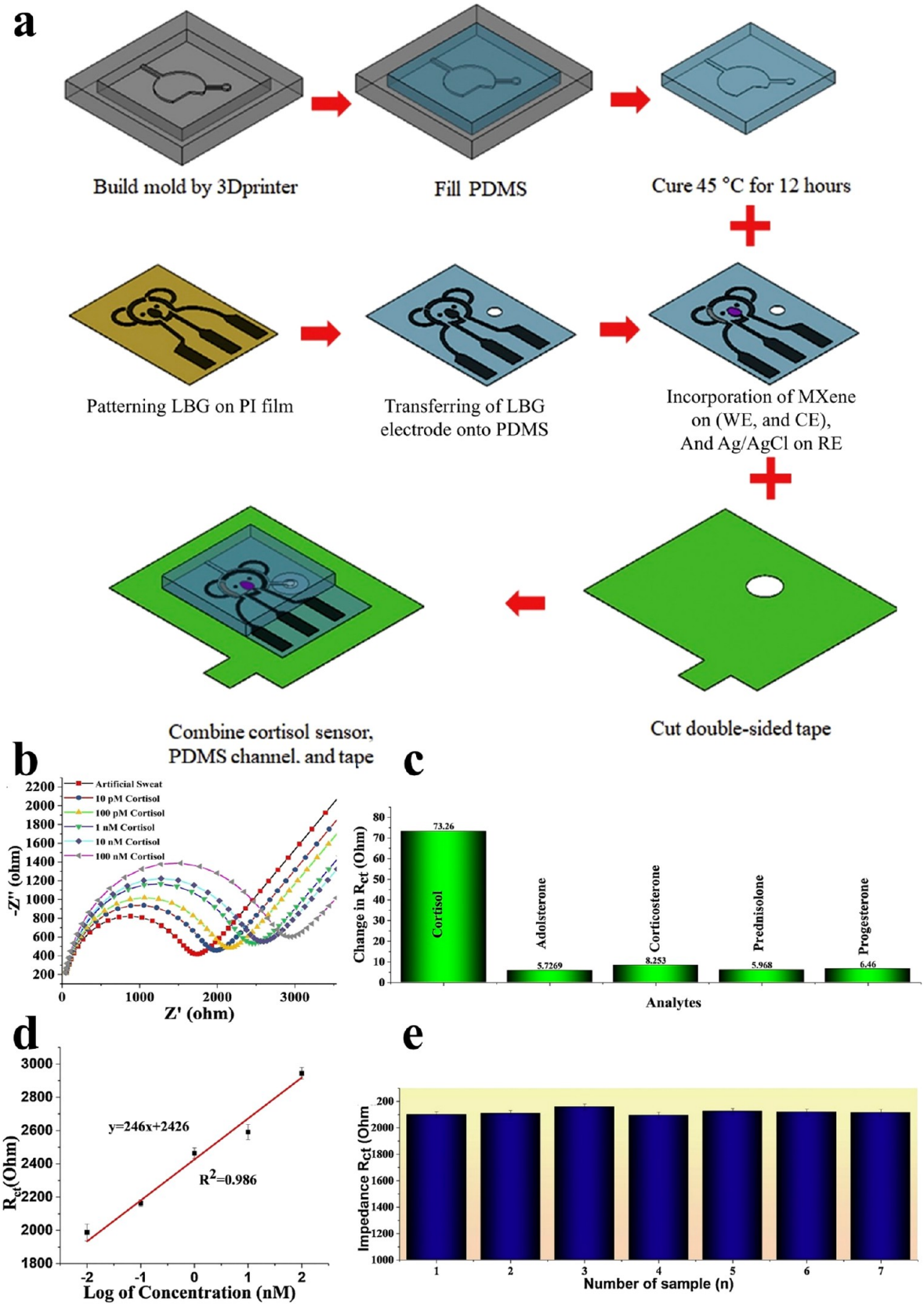

Figure 3. (a) Schematic illustration of wearable patch cortisol sensor integrated with a microfluidic system, (b) EIS method assisted cortisol biomarker detection, (c) corresponding linearity, (d) selectivity assessment in the presence of progesterone, prednisolone, corticosterone, and aldosterone, and (e) analysis of reproducibility. Reproduced with permission from ref 54. Copyright 2021 Elsevier.

perspectives and potential applications centered around MXene microfluidics.

MXenes arise from the exfoliation of ternary carbide and nitride ceramics, boasting a generalized formula represented by

https://doi.org/10.1021/acsbiomaterials.3c01361
ACS Biomater. Sci. Eng. 2024, 10, 657−676

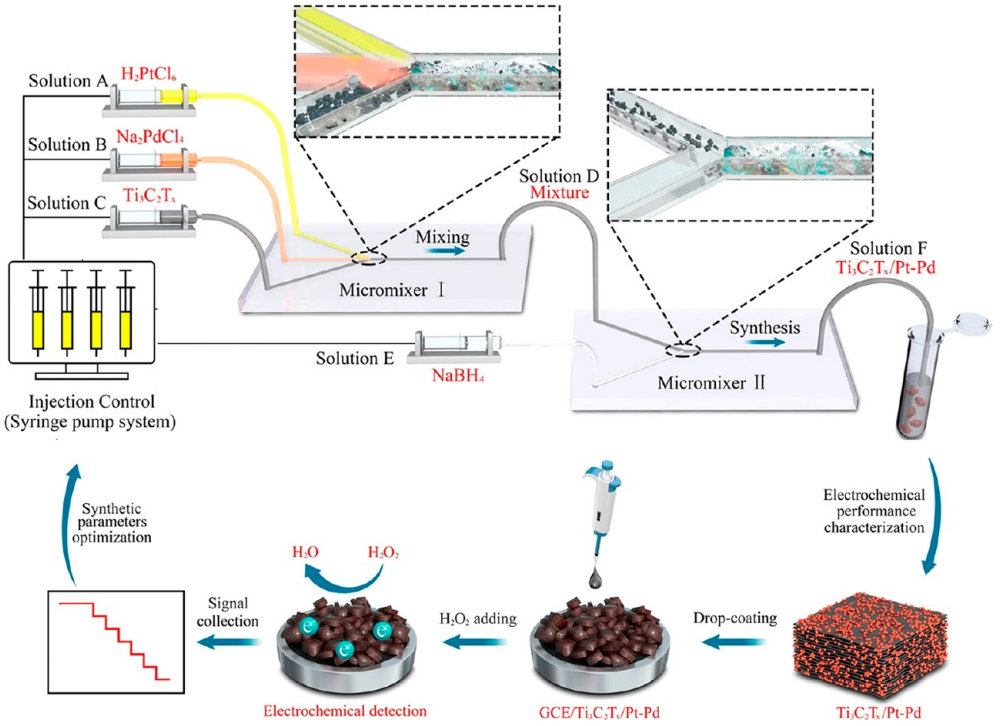

Figure 4. Microfluidic synthesis platform schematic illustration and H_2O_2 sensing procedure. Reproduced with permission from ref 55. Copyright 2022 American Chemical Society.

$M_{n+1}X_nT_x$, where n can be 1, 2, or 3 (as shown and described in Figure 2). In this equation, M characterizes a transition metal, X signifies nitrogen and/or carbon, T denotes surface groups, and x represents the matching number.[41,46,47] At present, a collection of over 70 MXene variants has been established.[48,49] Among these, Ti_3C_2 stands out as one of the extensively explored members within diverse fields like pollutant management, ion batteries, supercapacitors, antibacterial applications, and tumor treatment, among others. The integration of MXene has the potential to address prevailing limitations in continuous sensing while broadening the range of sensor applications.[50−53] For instance, Nah et al. designed a wearable microfluidics-integrated immunosensor to detect sweat cortisol noninvasively. They developed a cost-effective and one-touch system and based on their report, their fabricated $Ti_3C_2T_x$-based immunosensor revealed applicability in the dynamic range of 0.01−100 nM and limit of detection of 88 pM (Figure 3).[54]

The potential of MXene arises from several key factors. (i) The accordion-like multilayer structure seen in MXenes like $Ti_3C_2T_x$ provides a substantial surface area that is well-suited for tasks such as target detection, enzyme incorporation, and electrocatalytic reactions. (ii) The exceptional physical and chemical properties of MXenes offer a means to address potential stability challenges that could otherwise emerge. (iii) The inherent abundance of surface groups in MXene allows for bonding or adsorption of additional biorecognition elements, thereby heightening the signal responsiveness. (iv) Both the prior explorations and the current study affirm the robust resistance of MXene to passivation and fouling. (v) The established biocompatibility of MXene is evident through enzymes that can effectively adorn its surface, thus ensuring the prolonged activity of enzymes, and thereby securing sensor stability. (vi) The favorable electrical conductivity intrinsic to MXene renders it a superb choice for enhancing the capabilities of electrochemical sensors. These individual attributes show that the potential relationship between microfluidic technology and the porosity of MXenes could be established for various applications and material synthesis. As a matter of material applications, MXenes with controlled porosity can be utilized with microfluidics. For instance, they can be utilized for the preparation of porous films or scaffolds. In the case of material synthesis, although the conventional synthesis procedure requires harsh conditions, microfluidic technology could potentially be used for the synthesis of MXenes and to control the porosity of MXenes during their synthesis. Microfluidic technology provides a cost-effective path by manipulating temperature, reaction time, flow rate, and other conditions that can directly influence the formation of the pores within an MXene structure.[55] The MXenes stacking layers are influential in their physicochemical properties such as their thermal, mechanical, and electronic behavior. Altering these criteria will affect the final performance when integrated into microfluidics. MXenes, these 2D compounds derived from their 3D counterparts (MAX phase). Selective etching of the 'A' element from the MAX phase leads to different layered structures with M and X atoms. Different configurations can be adopted by stacking these layers (ABA and ABC) which leads to different features. The energetic stability of the ABA and ABC stacking of MXenes can vary through changes in the energetic barrier (Eb) and reaction step energy (ΔE). These criteria can be altered when the sample is exposed to different conditions in microfluidics. It is reported that various ions or molecules intercalation among MXene layers can also interchange the stacked atomic layers properties.[56] For instance, the intercalation of NH_4^+ and NH_3 during the MXenes delamination procedure led to uniformly spaced stackings. The fluid flow controllability through microfluidics can provide more consistent and predictable responses.[57] As an example, Liu et al. have produced a high throughput

https://doi.org/10.1021/acsbiomaterials.3c01361
ACS Biomater. Sci. Eng. 2024, 10, 657−676

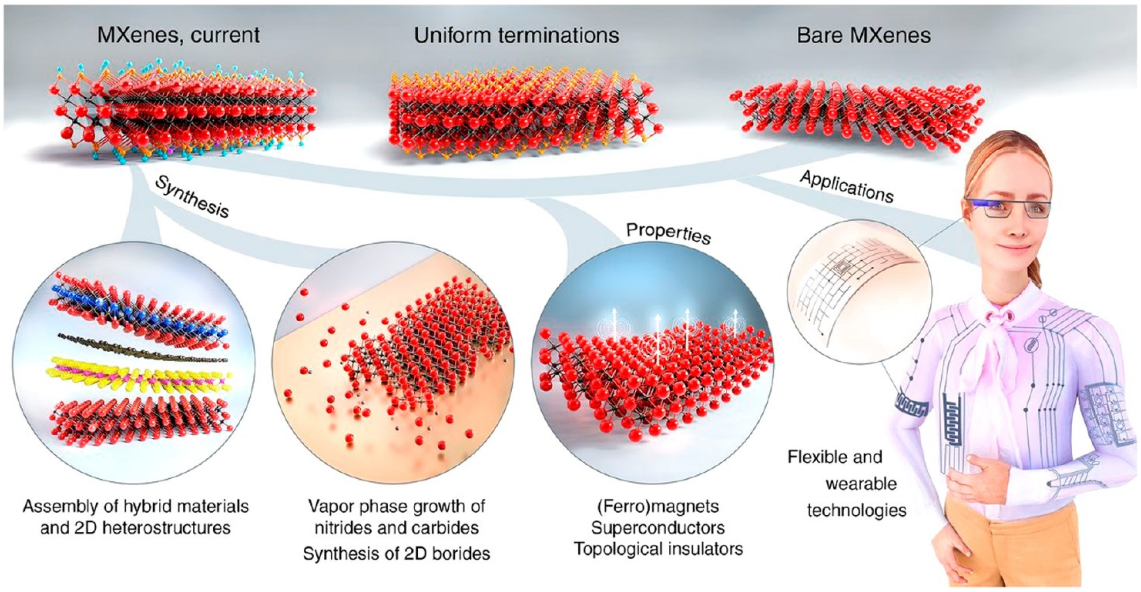

Figure 5. Schematic illustration of the structural design and synthesis of MXene. The exploration of novel MXene configurations and formulations, along with the precise management of their surface modifications, coupled with their integration with other 2D materials in 2D heterostructures and superlattices, holds the potential to introduce fresh characteristics and broaden the application scope of MXenes across diverse domains. They can be used in actuators, sensors, optical components, artificial memory devices, quantum computers, and Internet of Things (IoT) technologies, among many other applications. Reprinted (reproduced) with permission from ref 45. Copyright 2021 Science.

microfluidic platform for synthesizing $Ti_3C_2T_x$ highly efficiently continuously and at room temperature. They have utilized two micromixers which elements helically integrated into the microfluidics for enhancing the secondary flow to promote transfer and interactions during synthesis procedure. The aggregation has been prevented by rapid mixing and harsh vortices in 3D micromixers which also led to homogeneous distribution. The size controlled fabricated composites have been utilized as H_2O_2 sensor (Figure 4).[55]

2. WEARABLE MICROFLUIDIC-ASSISTED MXENES

The production of i-MXenes, which include structures featuring organized vacancies, such as Ti_4C_3, Ti_5C_4, and $Mo_4VC_4T_x$ MXenes, has been demonstrated. Additionally, there has been success in growing nanometer-thin Mo_2C through chemical vapor deposition (CVD).[58] Several solid solution MXenes have also been synthesized, and carbide MXenes have been transformed into nitrides through treatment in ammonia at elevated temperatures. Furthermore, the conversion of TMDs to 2D nitrides like Mo_5N_6 and W_5N_6 has been performed topochemically which indicates the potential for synthesizing many other 2D carbides and nitrides, and such explorations can be beneficiaries of high-throughput simulations and machine learning to expedite materials discovery.[59−61] Predictions and experimental endeavors have expanded beyond MXenes, encompassing diverse 2D structures with distinct chemical compositions. This includes 2D MC_2 carbides, such as TiC_2 (subject to pending experimental confirmation), ultrathin MAX phases (commonly known as MAXenes), vapor-grown 2D $MoSi_2N_4$, and a nascent category referred to as 2D borides (referred to as MBenes)[62−64] which shares a formula akin to MXenes wherein boron is substituted for the X sites. Anticipations have materialized in certain cases, leading to the partial exfoliation of particles or the cultivation of ultrathin crystals within these structures. Electrides like carbide and nitride electrides, exemplified by Ca_2N, have garnered attention due to their appealing physical properties despite their limited environmental stability.[65] For instance, 2D $MoSi_2N_4$ produced in a gas, has a remarkable Young's modulus of about 0.5 TPa and a breaking strength of about 66 GPa.[65] Density functional theory (DFT) calculations offered insights into a diverse array of semiconducting two-dimensional (2D) structures characterized by the general formula MA_2Z_4 wherein M signifies a transition metal, A can be either Ge or Si, and Z exhibits variations in the form of N, P, or As. Furthermore, computational predictions have illuminated the promising potential of 2D MC_2 carbides, including materials such as NbC_2, TaC_2, and MoC_2, across a wide spectrum of applications spanning from biomedical sciences to catalysis, encompassing tasks like the oxygen evolution reaction (OER) and hydrogen evolution reaction (HER) (Figure 5).[66−69] Partially etched borides have emerged as promising candidates for electrocatalytic HER applications. In a fashion analogous to MAX phases, the bonds between M and A elements in MAB phases exhibit a lower strength relative to M−B bonds, suggesting the possibility of discerning etching of A-elements. Nevertheless, prior attempts have yielded multilayer MBenes, where periodic elimination of aluminum layers resulted in stacking faults comprising a single aluminum layer, thereby impeding further deintercalation and exfoliation. Consequently, further research is imperative to pinpoint suitable precursors and attain the thorough exfoliation of MAB phases into MBenes.[70−73]

For the first time, an electrochemical system comprised of microfluidic channels and chambers impedimetric immunosensor has been created for noninvasive monitoring of the cortisol biomarker in sweat of humans.[54] The sensor employed in this study featured a three-dimensional (3D) electrode network composed of laser-burned graphene (LBG) flakes loaded with $Ti_3C_2T_x$ MXene wherein the polydimethylsiloxane (PDMS) substrate enabled the fabrication of this elastic and flexible patch sensor. By removal of the polyamide (PI)

https://doi.org/10.1021/acsbiomaterials.3c01361
ACS Biomater. Sci. Eng. 2024, 10, 657−676

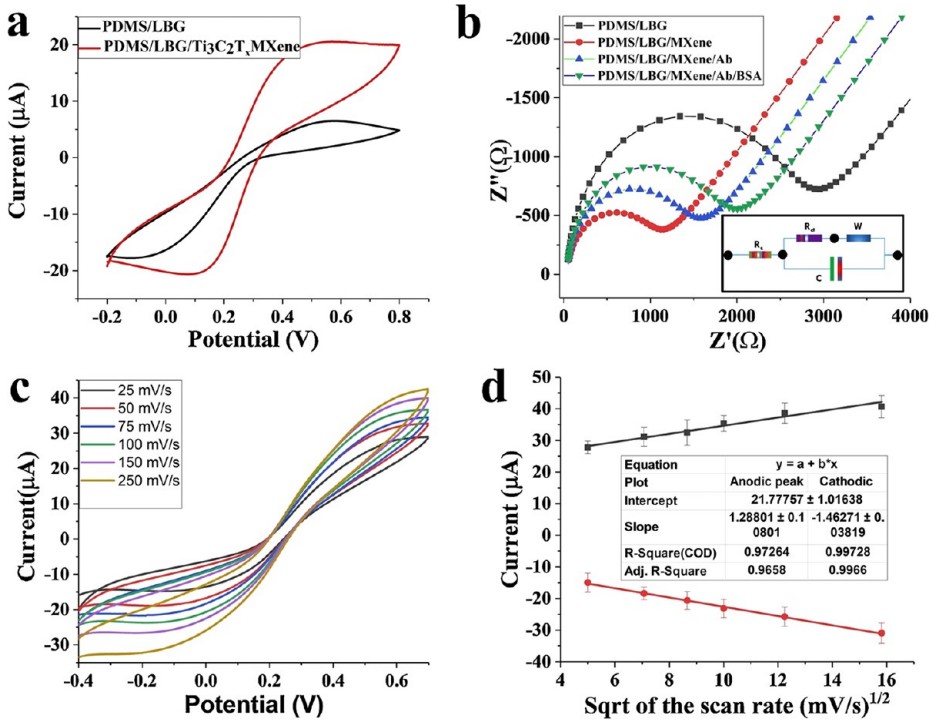

Figure 6. Cortisol sensor was systematically evaluated through the following procedures: (a) cyclic voltammetry (CV), (b) electrochemical impedance spectroscopy (EIS), (c) diffusion-controlled analysis spanning a range from 25 to 250 mV/s, and (d) determination of the corresponding linear relationship. Reproduced with permission from ref 54. Copyright 2021 Elsevier.

covering, LBG could be transferred to the PDMS substrate. During this process, an intentional gap was created by laser burning, resulting in disconnections between the laser-burned graphene flakes, which in turn led to a reduction in the LBG electrode's efficiency as an electrochemical device. To mitigate this issue of interflake disconnection arising from the burning and transfer procedures, the electrode was enriched with highly conductive $Ti_3C_2T_x$ MXene. The microfluidic system proposed in this study was created by using a 3D-printed mold and PDMS, enabling the attachment of the sensor to the skin. Sweat was collected and naturally transported through the channel to the chamber through inherent pressure mechanisms. The effective incorporation of $Ti_3C_2T_x$ MXene was validated through various techniques, including XPS (X-ray photoelectron spectroscopy) and FESEM (field emission scanning electron microscopy) (FESEM). Under optimized parameters, the cortisol immunosensor constructed using $Ti_3C_2T_x$ MXene/LBG/PDMS displayed a linear response and achieved a detection limit of 0.01−100 nM and 88 pM, respectively (Figure 6). Based on the comprehensive examinations conducted, it can be inferred that the devised methodology is suitable and versatile for the point-of-care detection of cortisol biomarker.

In another work, an innovative electrochemical sensor patch system was developed to constantly scrutinize the concentration of (K^+) in human sweat in real-time. This system is ultrasensitive, adaptable, wireless, battery-free, and entirely integrated.[74] The system comprises a microfluidic unit designed for on-site sweat collection applications. It employs a hybrid multidimensional network, combining multiwalled carbon nanotubes (MWCNT) and MXene-$Ti_3C_2T_X$, to establish a highly activated surface area, thus promoting rapid charge transfer and ensuring effective adsorption of the valinomycin membrane. This approach effectively shields the ionophore and facilitates the efficient transport and immobilization of potassium ions ($[K^+]$). Accelerated ion diffusion kinetics is further enhanced by the regulated porosity of carbon-based materials. When deployed for the detection of low concentrations, this novel hybrid nanonetwork topology greatly improves electrochemical stability and sensitivity by eliminating noise and signal drift. The developed sensor exhibits notable sensitivity to ion concentration, initially at a rate of 63 mV/dec, which is further enhanced to 173 mV/dec through an integrated amplification system ensuring exceptional selectivity. The sensor's measurements are wirelessly transmitted to a smartphone via Near Field Communication (NFC). To optimize sweat collection from the surface of the skin and minimize sensor contamination, a microfluidic channel is seamlessly combined with the electrochemical sensor patch. Moreover, the adaptable nature of the sensing patch enables its usage for on-site detection of various other biomarkers. One approach to achieving this goal is by integrating selective membranes tailored for specific biomarkers onto the working electrode. Within the NFC chip, the SD14 module houses a multichannel sigma-delta analog-to-digital converter, boasting a remarkable 14-bit resolution. Additionally, the NFC chip is equipped with both a programmable gain amplifier (PGA) and a sigma-delta analogue-to-digital converter (ADC) (Figure 7).

The $[K^+]$ sensor's output was captured via a 14-bit ADC converter. Subsequently, a dedicated smartphone appliance was established using Android Studio software to interpret and calibrate the ADC's output voltage, presenting it as the $[K^+]$ concentration. The NFC sensor system was initiated wirelessly using RF power supplied by the smartphone. Upon approaching a smartphone, the sensor system's compatibility with NFC protocols is detected. After being instructed to begin analog-to-digital converter (ADC) conversions for rectified

https://doi.org/10.1021/acsbiomaterials.3c01361
ACS Biomater. Sci. Eng. 2024, 10, 657−676

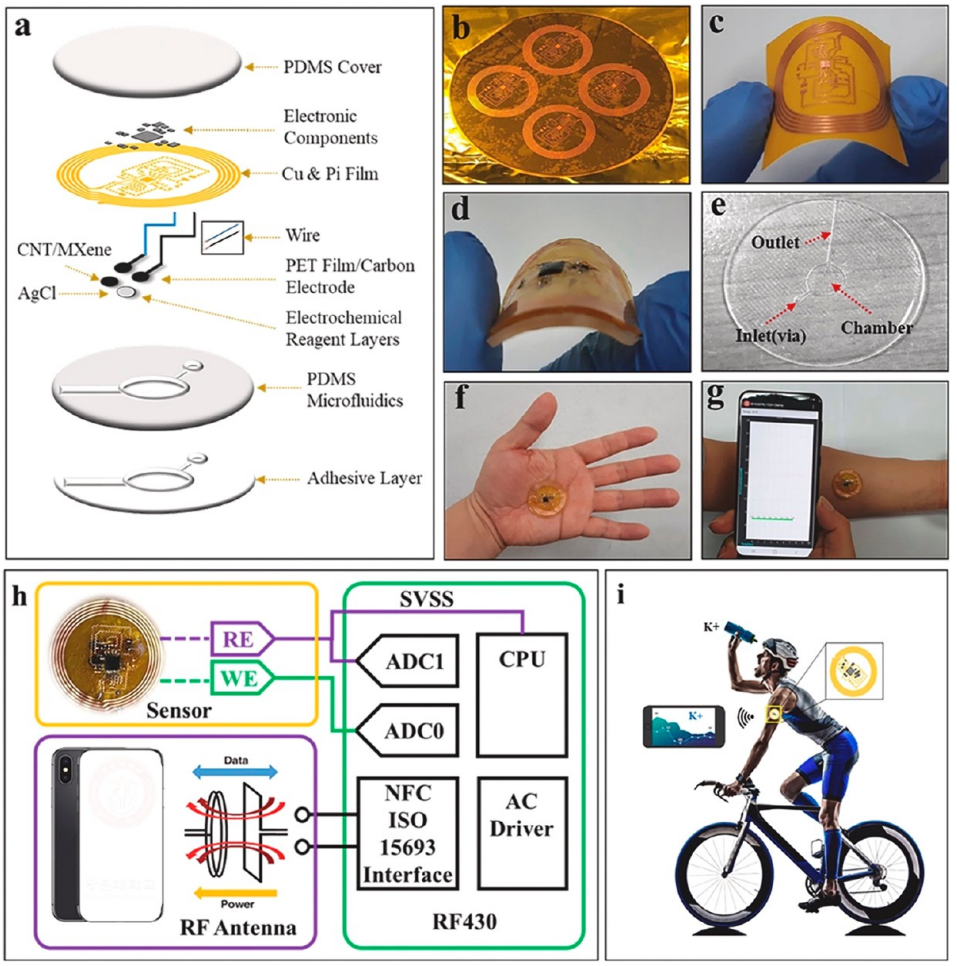

Figure 7. (a) This diagram provides an overview of the individual components that constitute the battery-free, wireless, and flexible microfluidic/electronic system. (b, c) The flexible antenna and circuits are crafted using a process involving lithography and etching techniques. (d) For safeguarding purposes, the flexible circuits are enclosed within PDMS (polydimethylsiloxane). (e) The microfluidic system is presented in detail. (f) Demonstrated here is an exceptionally lightweight and compact circular patch sensor system, boasting a 3.3 cm diameter. (g) The system showcases real-time wireless NFC sensor communication with smartphones. (h) This comprehensive setup encompasses electronics design, a measurement strategy, and an all-inclusive arrangement for experimentation. (i) Analyzing electrolyte losses from athletes' sweat has the potential to assist healthcare professionals in devising individualized water and electrolyte replacement plans. Reproduced with permission from ref 74. Copyright 2021 Elsevier.

voltages, the device also sounds an auditory prompt tone to denote the start of data exchange and subsequently sends the potential value correlating to the $[K^+]$ concentration wirelessly to the smartphone. The sensor operates within a two-electrode system and is powered electrochemically, thus eliminating the requirement for batteries or other external power sources. Between the electrodes, the sensor produces a potential of 100−400 mV in response to $[K^+]$ concentration fluctuations in the range of 1 to 32 mM. In order to increase the standing voltage source (SVSS) voltage to ∼125 mV above ground, the working electrode (WE) is linked to an ADC interface, while the reference electrode (RE) is connected to the SVSS. This adjustment mitigates minor inaccuracies stemming from the ADC's nonlinear behavior near ground potential. To effectively represent the potential range of the $[K^+]$ sensor, extending from 100 to 400 mV, the NFC chip configuration incorporates cascaded integral comb filtering applied to the sampled data (Figure 7). In order to decrease background noise, this method uses an extraction ratio of 256. The status register is programmed to indicate when data sampling is complete, and data is ready during continuous data readings.

Continuous monitoring of glucose levels in sweat using wearable noninvasive sensors holds great promise for the management and treatment of diabetes. However, the efficient development of such sensors faces obstacles related to glucose catalysis and the collection of sweat samples. In a separate study, researchers have presented a novel electrochemical sensor that is both flexible and wearable, enabling the continuous and nonenzymatic detection of glucose in sweat[75] wherein Pt nanoparticles and MXene ($Ti_3C_2T_x$) nanosheets were combined to make a catalyst termed Pt/MXene. Under neutral circumstances, this catalyst demonstrated a broad linear range for glucose detection (0.0−8 mmol/L). The structure of the sensor was optimized by immobilizing the Pt/MXene catalyst in a conductive hydrogel, which greatly increased its stability. By incorporation of a microfluidic patch onto the sensor for sweat collection, a wearable glucose sensor with this optimal shape has been developed. The sensor was evaluated for its ability to detect glucose levels in sweat, and it successfully detected changes associated with the body's energy replenishment and consumption, similar to changes in blood glucose levels. *In*

https://doi.org/10.1021/acsbiomaterials.3c01361
ACS Biomater. Sci. Eng. 2024, 10, 657−676

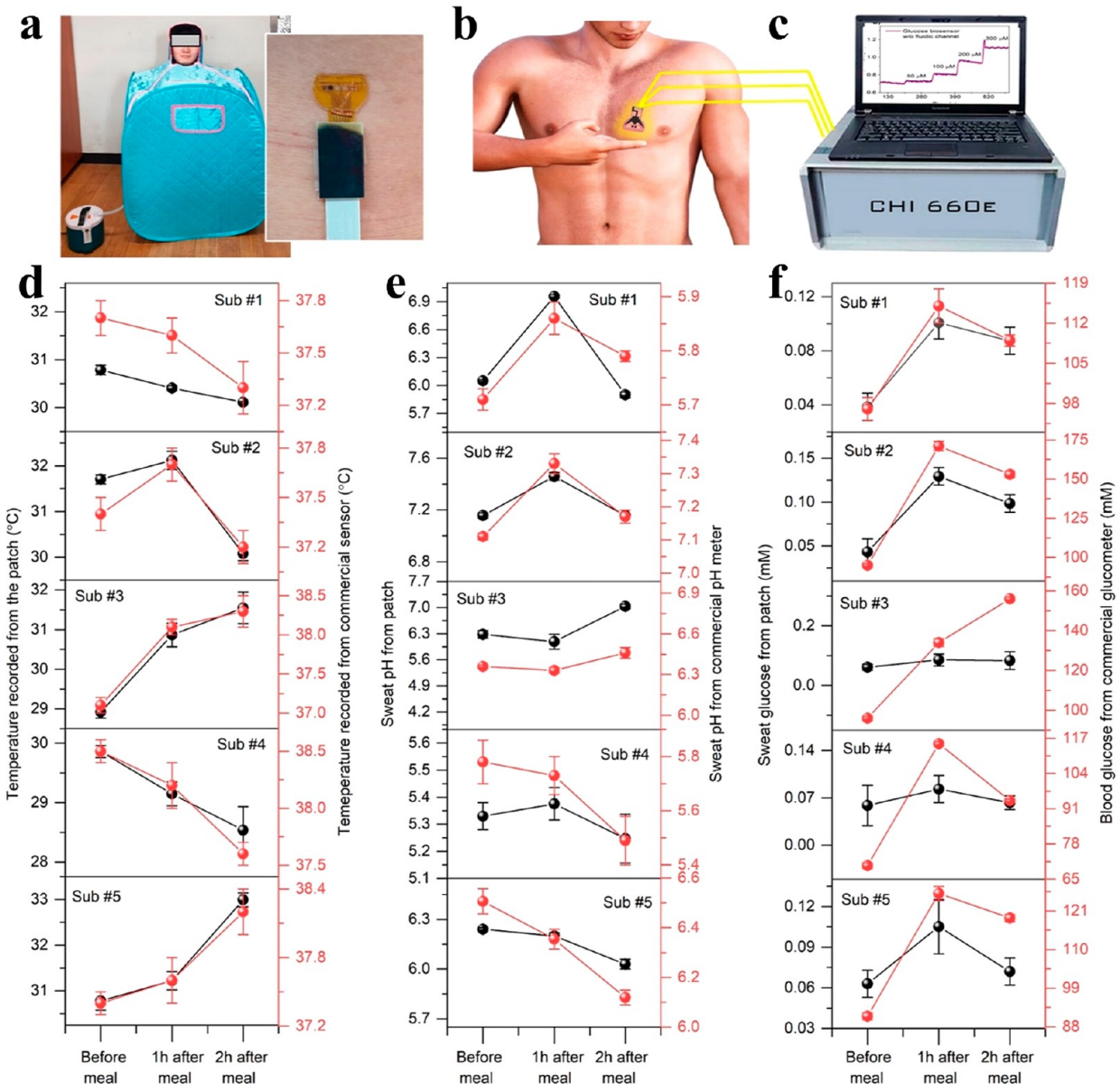

Figure 8. Chemical and temperature-sensitive patch was subjected to real-time on-body assessment involving five participants in three distinct scenarios: premeal and at 1 and 2 h after meal. This assessment utilized an electrochemical workstation. (a) Seated participant donning a sweat gown, which promotes the generation of sweat. (b, c) Diagrams elucidate the data collection process for glucose, pH, and temperature concerning evaluation of the patch. (d) Simultaneous temperature readings near the patch were obtained by using both the developed sensors and commercially available counterparts for comparative analysis. (e) Sweat pH measurements were concurrently taken deploying the custom biopatch and a traditional pH meter, allowing for a side-by-side comparison. (f) The association between the sweat and blood glucose levels was concurrently established using the devised patch and a glucometer. Reproduced with permission from ref 76. Copyright 2023 American Chemical Society.

vivo testing on sweat demonstrated the potential of the sensor for continuous glucose measurement, which is crucial for diabetes treatment and management. While wearable monitoring systems have made significant advancements, many designs primarily focus on detecting physical parameters or metabolites, without considering the combination of miniaturization, multimodality, and microfluidic channels. However, in another study, researchers developed a patch-based wireless system that addresses these limitations. This innovative system combines multimodal biosensing, encompassing both biochemical and electrophysiological measurements, with the integration of microfluidic channels. By incorporating these features, the researchers have created a comprehensive and versatile monitoring system that offers a more holistic approach to track and analyze various physiological markers.[76] The system employs flexible materials to enhance wearability and user-friendliness, while also enabling continuous real-time monitoring capabilities. A microfluidic channel-integrated glucose biosensor, utilizing reduced graphene oxide, is developed that exhibits noteworthy sensitivity, with 19.97 μA mM^{-1} cm^{-2} (44.56 without fluidic channels) and being effective within physiological levels (10 μM−0.4 mM). The biosensor showcases commendable long-term stability and resistance to bending. The sensors within the patch undergo initial validation through real-time tests on sauna gown sweat with participation from five individuals, each perspiring three times.

https://doi.org/10.1021/acsbiomaterials.3c01361
ACS Biomater. Sci. Eng. 2024, 10, 657−676

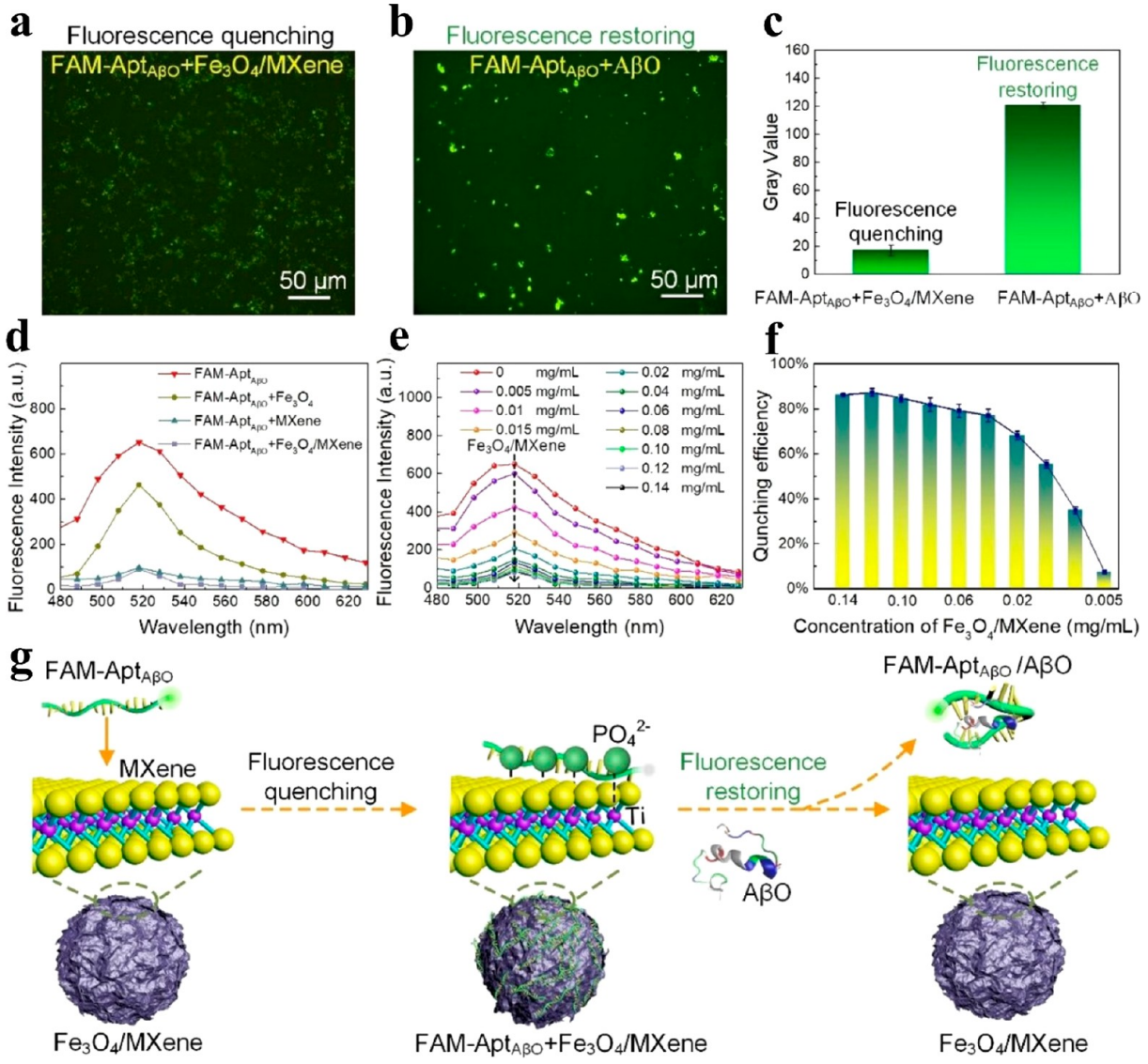

Figure 9. Exploring the fluorescence detection mechanism of 3D Fe_3O_4/MXene nanospheres: (a) Fluorescence image displaying FAM-AptAβO in the presence of Fe_3O_4/MXene. (b) Another fluorescence image featuring AptAβO together with AβO. (c) Histogram comparing the mean fluorescence intensities between FAM-AptAβO+Fe_3O_4/MXene and AptAβO+AβO. (d) Fluorescence intensities of pure FAM-AptAβO, FAM-AptAβO+Fe_3O_4, FAM-AptAβO+MXene, and FAM-AptAβO+Fe_3O_4/MXene conducted under uniform experimental conditions. (e) Fluorescence intensities of FAM-AptAβO across varying concentrations of Fe_3O_4/MXene. (f) Statistics on the efficiency of fluorescence quenching by Fe_3O_4/MXene at various concentrations. (g) Offers a schematic depicting the process of fluorescence quenching and restoration involving FAM-AptAβO. Reproduced with permission from ref 77. Copyright 2022 American Chemical Society.

The system outlined here integrates multimodal glucose and electrocardiogram (ECG) sensing, employing continuous adjustments in response to fluctuations in sweat pH and temperature to improve the precision of the measurements. To maintain minimal skin contact impedance (measuring at 40.5 kΩ cm^2), the ECG electrodes were created to achieve high-quality electrophysiological signals (signal-to-noise ratios of 23.4−32.8 dB). Laser-burned hierarchical MXene was coupled with poly(vinylidene fluoride) and conductive carbon nanofibers to create electrodes. To evaluate the system's performance, five patches were positioned on the chests of five participants during a real-time monitoring session. The participants wore a sauna gown to prompt sweat production, and the records, including sweat glucose and ECG readings, were collected wirelessly by using an electrochemical workstation. This methodology allowed for accurate and continuous monitoring of sweat composition and ECG data during physical exercise, providing valuable insights into the participants' physiological responses in real-time. Figure 8a depicts a participant seated in a sauna robe, with a patch securely attached to the chest. Approximately 5 min later, perspiration commenced, and it took an additional 5 min to completely fill the fluid channel. The procedure for measuring pH, temperature, and glucose using the electrochemical workstation is detailed in Figures 8b and c. This standardized procedure includes various steps, such as patch placement, meal composition, and sauna settings, which were maintained consistently for all participants. Before the patches were applied to the chest area, which was cleansed using alcohol-based swabs to ensure cleanliness, each patch underwent a stabilization process. Since pH and temperature are so important to precise measurements, they were measured

https://doi.org/10.1021/acsbiomaterials.3c01361
ACS Biomater. Sci. Eng. 2024, 10, 657−676

before the glucose detection to calibrate the sensor's response. The precision of the sensors was checked by comparing the results to those obtained from the standard pH and temperature meters. This procedure ensures that the measurements taken during the study are reliable and consistent across all participants, allowing for an accurate analysis and interpretation of the data. The average temperature of all participants is plotted in Figure 8d. Since rapid sweating could only be achieved thanks to the sauna suit's elevated temperature, measurements were above average (Figure 8d). Notably, the temperature data gathered from chest-placed biopatches differed from commercial data, which originated from earlobe measurements for each individual. This disparity was due to the commercial thermometer's capability to accurately measure earlobe temperature. Nevertheless, the congruence between temperature sensor data and commercial data trends validated the sensor's precision. Comparisons of pH data (Figure 8e) exhibited minimal fluctuation, and the process involved collecting sweat in a beaker and immersing the pH probe of the pH meter for measurement. On the other hand, the pH sensor integrated within the fluidic channel of the biopatch captured data instantly. The pH values obtained from the biopatch closely correlated with the readings from the pH meter, thus providing confirmation of its accuracy.

3. DIAGNOSIS OF DISEASES

The detection of Amyloid β protein oligomers (AβO) plays a crucial role in the diagnosis of Alzheimer's disease (AD). To meet the demand for a dependable method of detecting AβO, researchers have introduced an innovative fluorescent biosensor. This biosensor brings together FRET (fluorescence resonance energy transfer)-based fluorescence analysis with a microfluidic chip made from poly(dimethylsiloxane) (PDMS). By combining these elements, scientists aim to develop a reliable and efficient tool for early diagnosis and treatment of AD.[77] In this groundbreaking design, AO aptamers with a carboxyl fluorescein modification serve as the fluorophore while introducing Fe_3O_4/MXene nanospheres as a new type of fluorescence quencher, marking the first instance of combining these elements. The detection platform makes use of a PDMS-based multichamber microfluidic chip. Importantly, the biosensor exhibits a remarkable linear connection with the fluorescence intensity of the logarithm of the AβO concentration, ranging from 0.10 to 200 nM. Its detection limit stands at ∼0.05 nM, achieved with remarkably small sample volumes of only 4.50 μL. These outcomes underscore the exceptional performance of the engineered biosensor, rendering it suitable for a wide array of applications in the general domain of intelligent healthcare, encompassing medical diagnoses, health monitoring, and advanced biological research. The potential for DNA-based fluorescent detection is underscored by the inherent fluorescence quenching capacity and DNA adsorption capabilities exhibited by Ti_3C_2-MXene. In this work, the fluorescence emission from FAM-AptAβO is induced by a specific excitation wavelength. Subsequent exposure to Fe_3O_4/MXene results in a notable reduction in the fluorescence of FAM-AptAβO. However, the introduction of AβO leads to a restoration of the quenched fluorescence. As depicted in Figure 9a−c, the gray value of the FAM-AptAβO +AβO sample markedly surpasses that of the FAM-AptAβO+ Fe_3O_4/MXene sample. To further corroborate the fluorescence quenching phenomenon attributed to Fe_3O_4/MXene, FAM-AptAβO was subjected to incubation with MXene, Fe_3O_4, and Fe_3O_4/MXene under identical experimental settings. Subsequently, the fluorescence strength of these samples was assessed via a fluorescence microplate. As illustrated in Figure 9d, distinct peaks corresponding to FAM fluorescence at an approximate wavelength of 520 nm were identified. Following incubation with Fe_3O_4, there was a minor reduction in the fluorescence intensity of FAM-AptAβO, indicative of the slight fluorescence quenching capability of the Fe_3O_4 nanoparticles. Although Fe_3O_4 contributed to fluorescence quenching in this investigation, its effect was mitigated by MXene's encapsulation. Upon exposure to Fe_3O_4/MXene, a conspicuous decrease in the fluorescence intensity of FAM-AptAβO was discerned. Interestingly, the fluorescence strength of FAM-AptAβO +MXene was marginally higher relative to that of FAM-AptAβO+Fe_3O_4/MXene, attributable to the tendency of 2D MXene sheets to readily stack, thereby diminishing the effective surface area available for fluorescence quenching. These results affirm the primary function played by MXene in the process of fluorescence quenching, aligning with previously documented research.

In another study,[78] researchers have created a microfluidic chip that has been modified with hemin, resulting in the generation of dual electric signals for the precise finding of uric acid (UA); the addition of hemin serves as a catalyst and produces an inherent reference signal. To enhance the signal, attachment substrates, such as alkalinized titanium carbide (alk-$Ti_3C_2T_x$) and carbon nanotubes (CNT) are used. The collaborative impact of CNT, alk-$Ti_3C_2T_x$, and hemin together help to create an electrochemical sensor of remarkable proficiency, boasting advantageous catalytic activity and a distinct inherent signal capability. Scientists have undertaken extensive density functional theory calculations to comprehensively explore the interplay between the sensor's structural attributes, reactivity, and potential signal output mechanism. Subsequently, this functionalized sensor is seamlessly embedded into a microfluidic chip, resulting in the development of a portable electrochemical sensing platform. This platform empowers a sequential series of sample dispensation stages, including initial filtration, target enrichment, and dependable analysis. The enhancements made to the functionalized microfluidic platform have resulted in remarkable performance when determining UA, boasting a detection limit as low as 0.41 μM. Significantly, the platform has demonstrated precise UA detection in urine samples, representing a highly favorable avenue for biomolecule monitoring. The assessment of the platform was approached from two perspectives. Initially, it was deployed for the analysis of UA in serum specimens using the standard addition protocol. The results demonstrate that the recovery ratio falls within the range of 93.13% to 106.52%, affirming its practical applicability. Second, its application also lies in dietary management. Currently, there is a global rise in the burden of gout, influencing from different factors such as alcohol intake, genetic predisposition, certain medications, and excessive consumption of purine-rich foods, leading to elevated UA levels and potential gout attacks. A purine-rich meal was used to test the efficacy of the designed platform in diet administration, and urine specimens were obtained for analysis. In light of this, the UA strength in urine exceeded the maximum measurable value, necessitating a 2-fold dilution of the original samples prior to testing. Remarkably, UA levels rise following the consumption of a purine-rich diet and afterward decline over time. These outcomes are in strong agreement with those obtained from a commercial UA quantification kit,

https://doi.org/10.1021/acsbiomaterials.3c01361
ACS Biomater. Sci. Eng. 2024, 10, 657−676

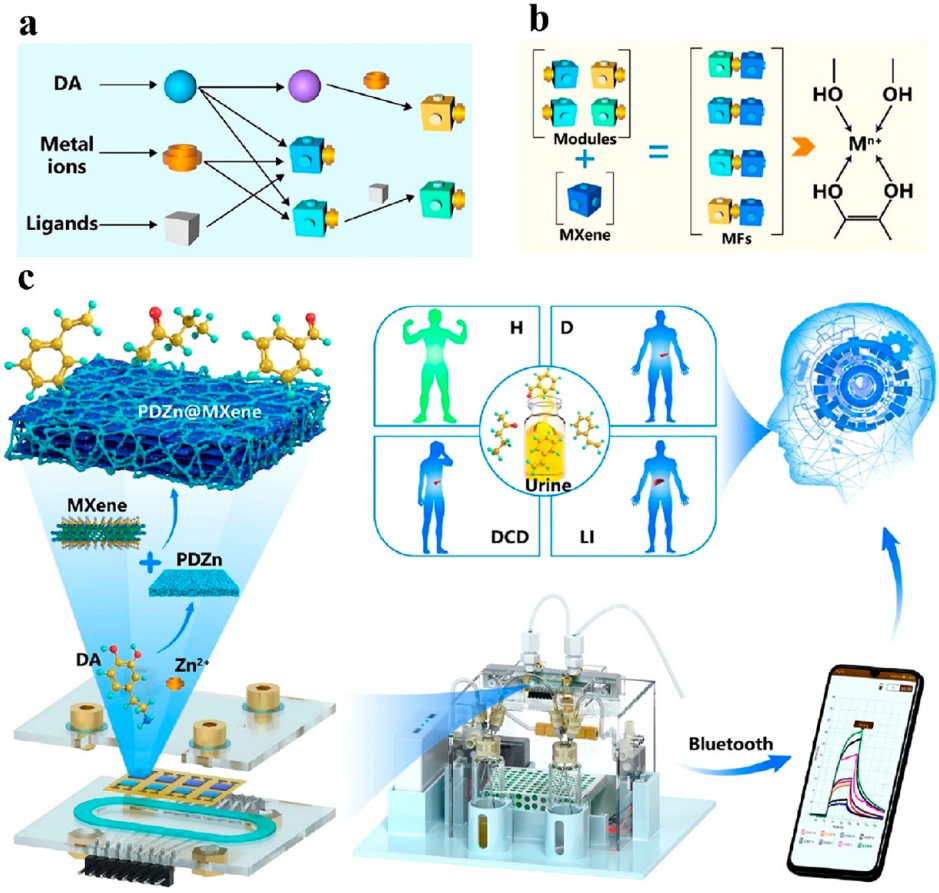

Figure 10. Modular assembly of MXene frameworks for noninvasive disease diagnosis via urinary volatiles. (a) The study focuses on the creation of adaptable modules utilizing dopamine, metal ions, and ligands through techniques involving metal ion doping, ligand engineering, and sequence regulation. (b) The modular assembly of porous MXene frameworks (MFs) is driven by coordination, involving the choice of modules and MXene, and the establishment of linkages between modules and MXene. (c) The development of the MHMF e-nose, and a portable POCT platform facilitates the monitoring of urinary VOCs for noninvasive disease diagnosis, with the assistance of machine learning ML techniques. Reproduced with permission from ref 79. Copyright 2022 American Chemical Society.

underscoring the platform's significant potential for UA monitoring. The research acknowledges the importance of VOCs (volatile organic compounds) in urine as valued biomarkers for noninvasive diagnosis of the disease. To address this, a straightforward strategy based on coordination has been utilized to construct a library of gas-sensing materials. The capability for detecting and analyzing VOCs has been a key feature of these materials, which are based on porous MXene frameworks (MFs).[79]

The MFs-based library, comprising a diverse range of modules with adjustable structures and varying compositions, has been developed to comprehensively address the needs of gas-sensing applications. Utilizing laser-prompted graphene interdigital electrode arrays and laser engraving microchambers, a microchamber-hosted MF (MHMF) electronic nose (e-nose) was successfully engineered. The MHMF e-nose boasts remarkable capabilities in pattern identification, allowing for concurrent detection and distinction of intricate volatile organic compounds (VOCs). What's more, the MHMF e-nose operates as a plug-and-play module, paving the way for the creation of a modular POCT (point-of-care testing) platform designed for real-time wireless scrutinizing of urinary volatiles in clinical specimens. Employing advanced machine learning techniques, this POCT platform achieves highly precise noninvasive diagnoses of a wide range of diseases, demonstrating an impressive accuracy rate of 91.7%. This development opens promising avenues for early disease detection, continuous monitoring of disease progression, and related research initiatives. As a proof-of-concept, a typical MF (PDZn@MXene) has been fabricated by employing MXene nanosheets and a coordination-driven assembly approach, resulting in a network structure interconnected by Zn^{2+}-anchored polydopamine (PDZn). (Figure 10). It was subsequently illustrated that modifications to metal components, chemical ligands, and their reaction sequences allowed for the creation of diverse modules, each possessing distinct compositions, structures, and functionalities, thus leading to the generation of a library of chemically tailored MFs with precisely defined attributes. Once prepared, MFs can be utilized as reservoirs of sensing materials that exhibit different responses to various VOCs.

A grid of LIGIE (laser-induced graphene interdigital electrodes) (in a 2 × 4 configuration) was manufactured using laser engraving technology to accommodate eight distinct MFs, facilitating the creation of a sensor array fabricated for the detection of VOCs. To optimize space utilization and maintain cost-efficiency, this sensor array was seamlessly integrated into a microchamber, resulting in the modular construction of a compact MHMF e-nose measuring dimensions of 5.44 cm in length, 4.50 cm in width, and 0.42

https://doi.org/10.1021/acsbiomaterials.3c01361
ACS Biomater. Sci. Eng. 2024, 10, 657−676

cm in height. The MHMF e-nose was conceived as a flexible chamber-sensor-on-a-chip capable of continuous monitoring of the chemiresistive reactions of MFs to diverse VOCs. The porous organization of the MFs, in conjunction with the microchamber's configuration, expedited swift response and recovery times, consistently achieving these within 1 min. Furthermore, this configuration showcased outstanding reversibility and heightened sensing prowess when exposed to various VOCs. Functioning as a versatile sensory tool, the MHMF e-nose exhibited substantial discrimination capabilities, enabling the simultaneous detection and pattern recognition of intricate VOC mixtures. Leveraging the MHMF e-nose as a recognizing component, a portable POCT system was assembled to analyze urinary volatiles in clinical samples related to health, diabetic comorbid depression (DCD), liver impairment (LI), and diabetes (D). Employing machine learning (ML) techniques, this developed POCT platform achieved noninvasive disease diagnosis with a remarkable precision rate of 91.7%, which may surpass most similar platforms' precision rates.

The simultaneous detection of multiple components with high sensitivity and selectivity is crucial in various applications, including environmental monitoring and healthcare. However, achieving this has been a long-term challenge, mostly because conventional sensors rely on a single sensing mechanism. To address this, researchers have utilized the benefits of microfluidic chips and SERS (surface-enhanced Raman spectroscopy). By combining these technologies, they have developed a smart single-chip solution that enables the simultaneous detection of any combination of VOCs. This advancement has the potential to revolutionize sensing capabilities and expand the range of applications for gas sensors.[80] This is achievable by incorporating different detection units that operate based on either a chemisorption or physisorption mechanism. Microfluidic components and multiplex nanostructures have been effectively integrated on a single chip, allowing for a tunable sensor design for a broad spectrum of volatile chemicals. On-chip signal amplification is made possible by this integration as well, which further improves reproducibility. A proof-of-concept experiment has been conducted that could identify nine different gases—including aromatic compounds, sulfides, ketones, and aldehydes—in a single mixture. Despite having an error rate of roughly 8%, this detection was remarkably sensitive to the parts per billion level, selective, and robust. The flexibility of this universal gas sensor was evaluated in two real-world settings: tracking interior air pollution and analyzing exhaled breath samples to identify disease. For SERS detection, a sensing area was configured as a 3 × 3 array, comprising three units termed UA, UB, and UC. Each unit featured three dots to minimize random errors. UA and UB utilized SERS substrates created using Au@Ag@Au nanocubes, coated with a layer of $Ti_3C_2T_x$ MXene to enhance absorption efficiency. In the case of UC, Au@Ag nanocubes were employed to facilitate the formation of Ag−S bonds. Using a colloidal self-assembly technique and a well-established tape-assisted substrate transfer strategy, this detecting array may be constructed with minimal effort.

The fabrication technique used in this study offers several advantages, including simplicity, speed, and cost-effectiveness, making it suitable for practical applications. By combining programmable detection units with various principles into a single chip, the detection of various gases such as aromatics, aldehydes, ketones, and hydrogen sulfide were rendered possible by deploying ordered 3D SERS substrates and generating vortices within the chip. The simultaneous achievement of high sensitivity at the parts per billion level, exceptional selectivity, and robustness (with an error rate of ∼8%) is hard to replicate with other gas sensor technologies. Indoor air quality monitoring and breath analysis were used to evaluate the sensor's universal gas detection capabilities. Despite complicated interferences, the results demonstrated the sensor's immense selectivity. The SERS-microfluidic technique has benefits, including portability, low cost, speedy reading, and scalability. It is also simple to increase the number of analyzable gases by switching out the gas-sensitive components. Changes in the SERS signal initiated by the realization of coordinating bonds among Fe(II) and CO allow for the detection of carbon monoxide when Dinitrophenylhydrazine (DNPH) is substituted with Fe(II) metalized 5-[(triisopropylsilyl)thio]-10,20-diphenylporphyrin (Fe-TDPP). In order to accelerate the creation of universal gas sensors for complex real-world samples, the research team proposes adopting programmable integrated chips as a strategy. This work may also inspire the development of data-driven applications in the field.

4. CUTTING-EDGE APPLICATIONS

Designing complex and advanced fibers with a vertical porous structure and significant electrochemical activity is essential for the advancement of high-performance fiber-shaped supercapacitors (FSCs) although this is a difficult task. Researchers have devised a solution to this problem by creating hybrid fibers with a predetermined hierarchy through a microfluidic synthesis process. These fibers combine vertically aligned and conductive $Ti_3C_2T_x$ MXene (VA-$Ti_3C_2T_x$) with interstratified electroactive COFs (covalent organic frameworks), LZU1 (COF-LZU1).[81] The generated VA-$Ti_3C_2T_x$@COF-LZU1 fibers showcase an impressive gravimetric capacitance of 787 F g^{-1} when assessed in a three-electrode setup. This remarkable performance owes itself to their distinctive attributes, encompassing vertical channels, electrodes with a variety of redox-active regions, and a huge portion of the exposed surface area. Furthermore, within solid-state asymmetric FSCs, these fibers demonstrate exceptional energy density (27 Wh kg^{-1}), capacitance (398 F g^{-1}), and a commendable cycling endurance of 20,000 cycles. These extraordinary energy storage capabilities stem from an improved distribution of charge density and a decrease in ion adsorption energy within the vertically aligned and active hybrid fibers. Such an arrangement expedites swift ion transportation, ensures efficient ion accommodation, and fosters effective interfacial electron transfer. Due to their exceptional electrochemical prowess, these FSCs deliver an abundant energy supply for a myriad of applications, including powering devices such as watches, flags, and digital display tubes. Additionally, they readily integrate with sensors for the detection of pulse signals. This technological advancement heralds promising prospects for advancing fiber technology in the carbon-neutral marketplace. In this study, the researcher introduced an innovative methodology for crafting hierarchical structures within a microfluidic wet-fusing spinning technique that is used to create MXene-based fiber fabrics (MFFs). This approach substantially enhances the versatility of MFF electrodes by imbuing them with extraordinary toughness, excellent conductivity, and improved machinability.[82] To

https://doi.org/10.1021/acsbiomaterials.3c01361
ACS Biomater. Sci. Eng. 2024, 10, 657−676

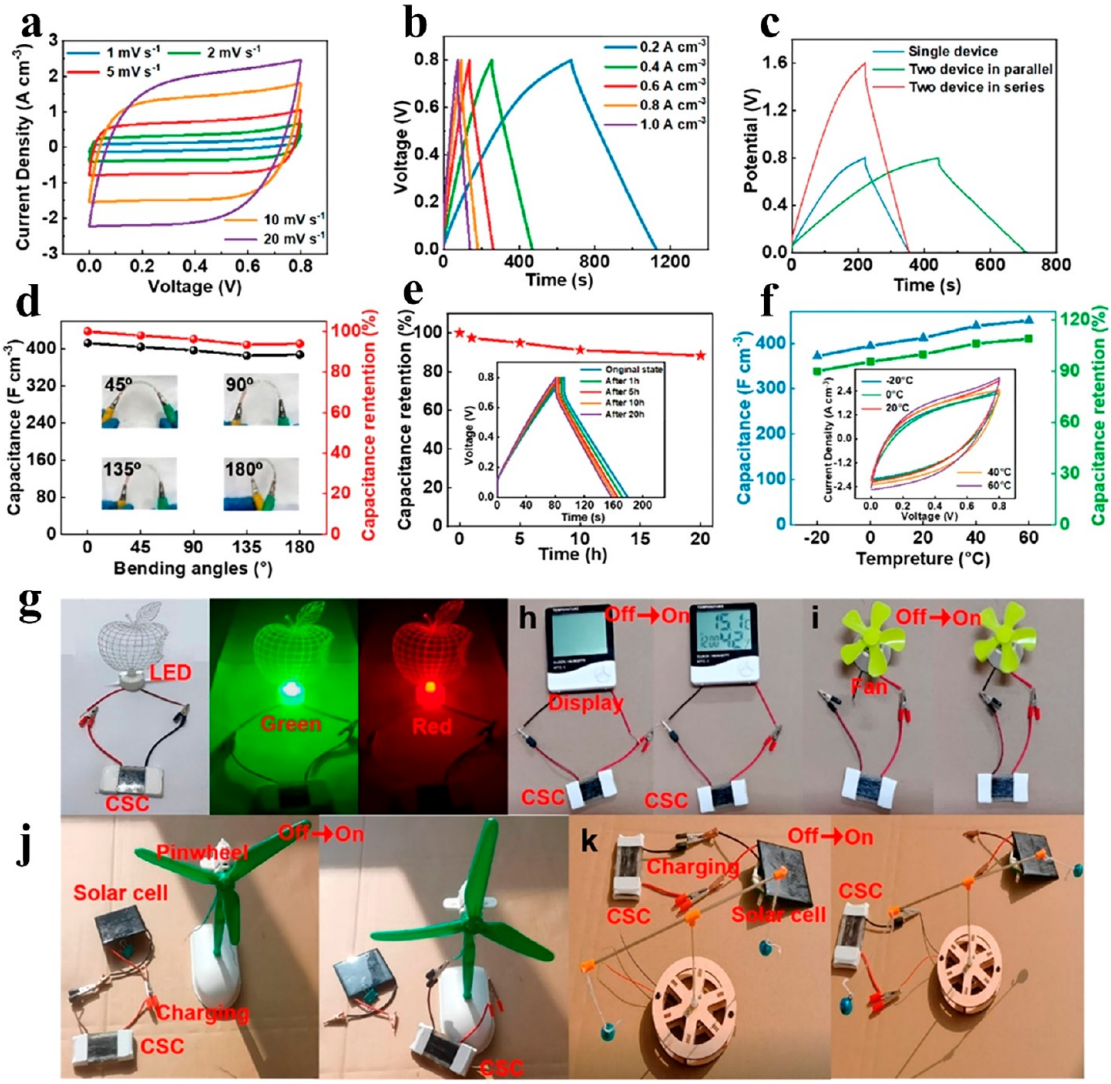

Figure 11. Electrochemical functioning of a solid-state ZIF-67@$Ti_3C_2T_x$ FSC is described as follows: (a) CV curves recorded at scan rates ranging from 1 to 20 mV s^{-1}. (b) Galvanostatic Charge−Discharge (GCD) curves were obtained at current densities varying from 0.2 to 1 A cm^{-3}. (c) GCD curves illustrate the performance of two FSCs when connected in both series and parallel configurations. (d) Assessment of the bending steadiness under various angles, accompanied by photographs depicting the FSC at different bending angles (inset). (e) Examination of motion stability over a duration of 0 to 20 h, with the corresponding GCD curves at a current density of 1 A cm^{-3} provided in the inset. (f) Capacitance retention and values were observed at different applied temperatures, with CV curves recorded at a scan rate of 20 mV s^{-1} shown in the inset. (g) Photographs of a capacitive supercapacitor (CSC) powering LED lights. (h) Photograph of a CSC deployed to power a display. (i) Photograph of a CSC driving an electric fan. (j) Photographs demonstrating a self-powered system using FSC to drive a pinwheel. (k) Photographs depicting a self-powered system employing FSC to activate a rolling bell. Reproduced with permission from ref 84. Copyright 2022 American Chemical Society.

improve the mechanical integrity of MXene fibers, a novel dot-sheet structure comprising MXene nanosheets and graphene quantum dots (GQDs) is employed within a microfluidic apparatus. These constituents engage in multiple anchor interactions within the microchannel. Subsequently, the integrated fiber network structure of $Ti_3C_2T_x$/GQDs fabrics is established through the MWSC process, thereby augmenting the fabric's flexibility. Lastly, a core−shell configuration, denoted as PANI@$Ti_3C_2T_x$/GQDs, is synthesized by fostering polyaniline (PANI) nanofibers through in situ polymerization. This architecture introduces additional pathways and sites conducive to ion migration and accumulation. By focusing on the optimization of morphology and microstructure, this method is endowed with significant implications for the scalable production of conductive fabric electrodes, as it offers a practical approach to enhance the mechanical endurance and electrochemical properties of these electrodes simultaneously. In this study, a Zinc(Zn) nanowall array sheath is raised vertically onto an anisotropic $Ti_3C_2T_x$ core by the establishment of TiOZn/TiFZn chemical linkages, yielding hierarchically ordered Zinc(Zn)@$Ti_3C_2T_x$ MXene core−sheath fibers.[83] Fully developed micro/mesoporosity, organized ionic routes, facilitation of rapid interfacial electron conduction, and the capacity for scaled-up manufacturing can all be attributed to the microfluidic assembly and microchannel reactions, which are extremely efficient processes. These improvements make charge transfer and intercalation much more efficient. The resultant ZIF−L(Zn)@$Ti_3C_2T_x$ fiber exhibits a substantial capacitance of 1700 F cm^{-3} and demonstrates exceptional rate performance when deployed in a 1 M H_2SO_4 electrolyte. Furthermore, solid-state asymmetric supercapacitors employing ZIF−L(Zn)@$Ti_3C_2T_x$ fibers exhibit impressive character-

https://doi.org/10.1021/acsbiomaterials.3c01361
ACS Biomater. Sci. Eng. 2024, 10, 657−676

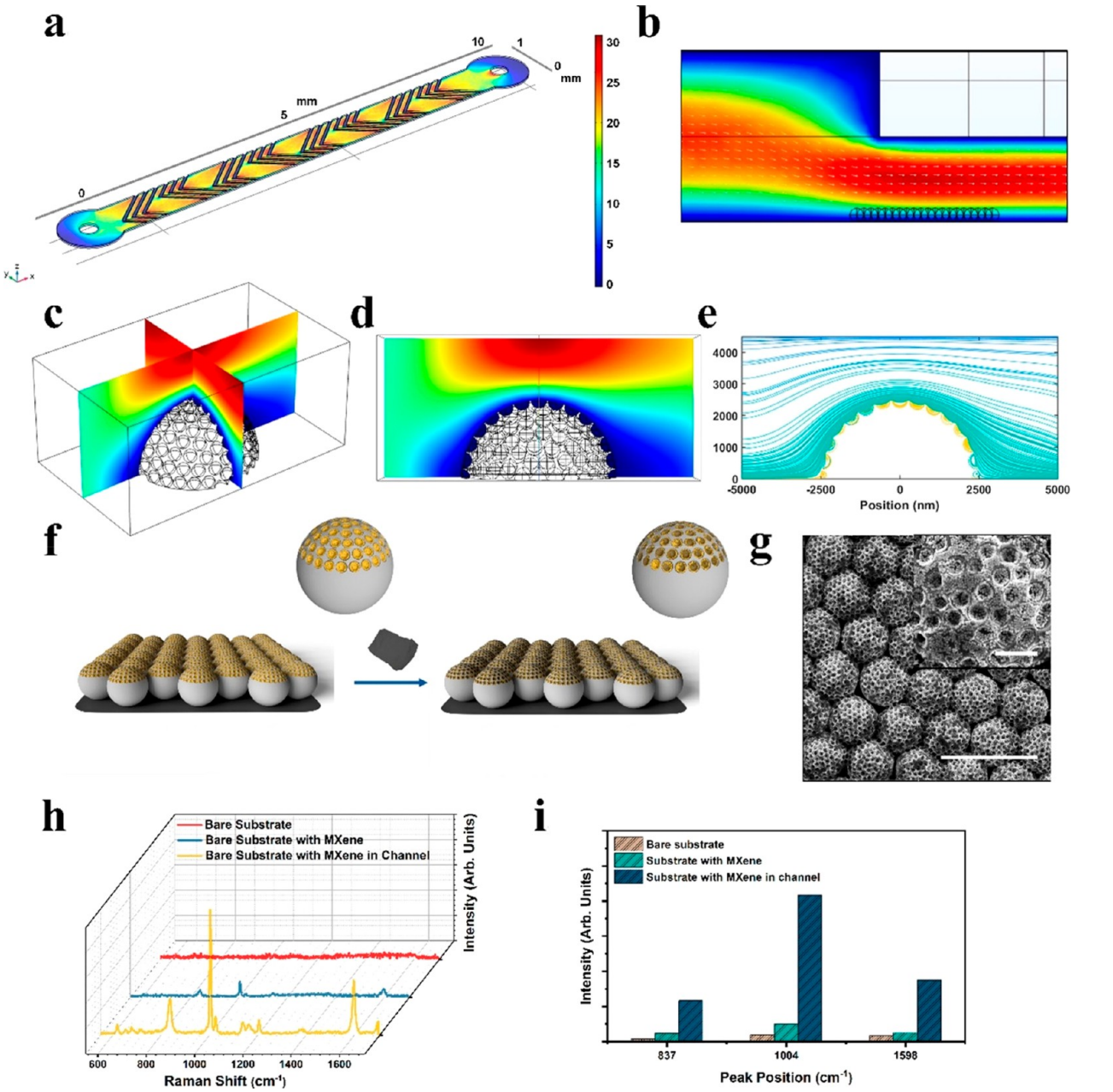

Figure 12. SERS-Vortexene chip was characterized and tested in several stages: (a) The herringbone chip's internal gas flow field simulation. (b) Channel near the deposited substrate side view. (c, d) Evaluating the gas flow field and (e) calculating streamlines near the substrate using simulation. (f) Visualizing the process of applying a monolayer $Ti_3C_2T_x$ MXene onto a bimetallic nanoparticle liner. (g) Scanning electron microscope (SEM) images. The scale bar in the SEM image inset represents 1 μm. (h) Presenting the SERS signals obtained for benzaldehyde under various testing conditions. The results from the SERS-Vortexene chip are shown in the yellow spectrum. The herringbone chip's blue spectrum is consistent with data obtained from a substrate devoid of MXene. The red spectrum represents the control data obtained from a substrate without any coating. (i) Measuring the intensity of typical peaks of benzaldehyde under various testing conditions. Reproduced with permission from ref 85. Copyright 2021 American Chemical Society.

istics, including high energy density (measuring at 19.0 mWh cm^{-3}), excellent capacitance (854 F cm^{-3}), remarkable flexible and wearable properties, and long-lasting cyclic stability (withstanding 20 000 cycles). Water level and earthquake alarm devices can be powered by solar-powered applications in view of these characteristics.

For high-performance FSCs (fiber-based supercapacitors), a key factor is the sophisticated fabrication of heterostructured fibers with organized transport channels and porous frameworks that enable fast ion and electron kinetics. However, the restricted capacity of such FSCs to store energy has typically prevented their broad implementation. Fibrous restacking and insufficient interfacial charge transfer are blamed for this shortcoming. The porous ZIF-67 (zeolitic imidazolate framework-67) polyhedron shell is evenly packed onto a highly conductive $Ti_3C_2T_x$ core in this study utilizing a flexible microfluidic method, creating a well-ordered core−shell fiber[84] (Figure 11). The utilization of the ZIF-67@$Ti_3C_2T_x$ fiber results in the generation of an improved porous structure, the establishment of ordered porous pathways, endowed with a

https://doi.org/10.1021/acsbiomaterials.3c01361
ACS Biomater. Sci. Eng. 2024, 10, 657−676

larger exposed surface area, and the promotion of in situ interfacial electron transfer. This leads to exceptional volumetric capacitance (972 F cm^{-3}) and long-term cycling steadiness (with 90.8% capacitive preservation after 20,000 cycles) when the fiber is deployed in 1 M KOH electrolytes. The flexible solid-state ZIF-67@$Ti_3C_2T_x$ FSCs also exhibit consistent capacitance, robust bending and wearability, and reliable temperature-reliant performance. These supercapacitors are capable of providing reliable power to a wide range of electrical gadgets, including LEDs, electric fans, displays, pinwheels, and rolling bells, due to their exceptional electrochemical accomplishments. This discovery paves the way for realistic improvements in tiny energy technologies and intelligent electronics.

By fusing a transferable 3D SERS substrate with ultraflexible $Ti_3C_2T_x$ MXene, a SERS-Vortexene chip was developed to demonstrate concurrent and straight multiplex gas sensing (Figure 12).[85] The chip demonstrated exceptional sensing capabilities, including high sensitivity, the ability for multiplex detection, and reliable reproducibility. The increased sensitivity could be attributed to the gas vortices created by the 3D structure within the microfluidic channel, which results in a longer residence time for gas molecules as affirmed by control experiments and theoretical simulations. MXene materials contribute greatly to improved detection sensitivity due to their exceptional adsorption ability for VOCs. Multiplex detection was made possible by the use of complementary ligand switching (CLS) and visible SERS barcodes, thus fully harnessing the multiplex detection potential of the SERS technique. The multiplex detection of 2,6-dinitrotoluene (DNT), indole, and benzaldehyde was achieved on the device with an error rate of less than 9% and a detection limit as low as 10 ppb (Figure 12). This eliminates the need to compromise between the detection depth and the number of sensors deployed. Importantly, each of these techniques can be employed separately to further improve the detection rates. Furthermore, the SERS-Vortexene chip can generate a spectrum library for the identification of various VOCs and their mixed forms by combining the SERS fingerprint spectrum using MXene's robust universal adsorption properties. In order to facilitate the development of highly sensitive and versatile gas sensors, researchers have proposed the deployment of a SERS-Vortexene chip to increase the awareness of ultraflexible MXene and SERS-microfluidic technology. Also, this technique could be considered aligned with the Green Biomaterials principles.[86]

5. CONCLUSION AND FUTURE PERSPECTIVE

The integration of MXene materials with microfluidics can stand at the scientific innovation forefront, which can hold tremendous potential across diverse fields. This perspective explores the multifaceted synergy between MXenes and microfluidics, highlighting their combined strengths in material science, sensing, energy storage, and biomedical research. It is crucial to acknowledge and address precise obstacles which currently hinder the potential applications of the integrated MXene microfluidics systems when we delve into the future. Current challenges can be (i) overcoming microfluidics manufacturability and commercialization hampers, (ii) increasing the biocompatibility and biodegradability of MXene-based compounds, (iii) MXene production scalability can be another ordeal. To address these challenges, proposed approaches are as follows: (a) encourage interdisciplinary cooperations between industry and academia for bridging the gap academic results, commercially viable and practical devices, (b) investigation of scalable biocompatible fabrication methods to ease the adoption of MXene microfluidic technique, (c) based on the scientific fact, preparation of tailored MXene-based compounds can be achieved through composite and functionalized derivatives, and (d) the optimization of MXene composition with other compounds is crucial for real time applications which need multiplexing sensing systems. Looking forward can illustrate that several key trends and opportunities can emerge, including the following: (i) Advanced materials development: Continued research on MXene synthesis and modification techniques will undoubtedly yield new materials with tailored properties, enabling even more versatile applications within microfluidic systems. These advancements may include MXene-based nanocomposites, hybrids, and functionalized MXene derivatives, thus expanding the range of possibilities for microfluidic devices. (ii) Enhanced sensing capabilities: MXene-based sensors integrated into microfluidic platforms hold the potential for ultrasensitive and selective detection of various analytes. (iii) Energy and environmental applications: MXene's unique electrical and electrochemical properties make it an ideal candidate for energy storage and conversion systems. Microfluidic devices could facilitate the development of more efficient and compact energy storage devices, namely, microsupercapacitors, batteries, and fuel cells. Furthermore, MXene-based membranes may find applications in water purification and desalination within microfluidic setups. (iv) Biomedical advancements: MXenes show promise in drug delivery, biosensing, and tissue engineering. Future perspectives in this domain may entail the development of biocompatible MXene-based microfluidic systems that can precisely control drug release, provide rapid and sensitive diagnostics, and create tailored environments for cell culture and tissue regeneration. Finally, as the MXene microfluidics integration assures transformative progress, the path toward success necessitates concerted actions for overcoming above-mentioned issues. This study strived to focus on innovations and practical examples to shed a light on the proposed path and pave the way toward the technological landscape where MXenes and microfluidics will collectively eradicate the complex challenges.

AUTHOR INFORMATION

Corresponding Authors

YunSuk Huh − *NanoBio High-Tech Materials Research Center, Department of Biological Sciences and Bioengineering, Inha University, Incheon 22212, Republic of Korea*; Email: yuksuk.huh@inha.ac.kr

Majid Ebrahimi Warkiani − *School of Biomedical Engineering, University of Technology Sydney, Ultimo, New South Wales 2007, Australia; Institute for Biomedical Materials and Devices (IBMD), University of Technology Sydney, Sydney, New South Wales 2007, Australia;* orcid.org/0000-0002-4184-1944; Email: majid.warkiani@uts.edu.au

Navid Rabiee − *Centre for Molecular Medicine and Innovative Therapeutics, Murdoch University, Perth, Western Australia 6150, Australia; School of Engineering, Macquarie University, Sydney, New South Wales 2109, Australia;* orcid.org/0000-0002-6945-8541; Email: nrabiee94@gmail.com

https://doi.org/10.1021/acsbiomaterials.3c01361
ACS Biomater. Sci. Eng. 2024, 10, 657−676

Authors

Moein Safarkhani − *NanoBio High-Tech Materials Research Center, Department of Biological Sciences and Bioengineering, Inha University, Incheon 22212, Republic of Korea;* orcid.org/0000-0001-7062-073X

Bahareh Farasati Far − *Department of Chemistry, Iran University of Science and Technology, Tehran 1684611367, Iran;* orcid.org/0000-0002-1598-2487

Eder C. Lima − *Institute of Chemistry, Federal University of Rio Grande do Sul (UFRGS), Porto Alegre CEP 91501-970 Rio Grande do Sul, Brazil*

Shima Jafarzadeh − *Centre for Sustainable Bioproducts, Deakin University, Waurn Ponds VIC 3217, Australia*

Pooyan Makvandi − *School of Engineering, Institute for Bioengineering, The University of Edinburgh, Edinburgh EH9 3JL, United Kingdom*

Rajender S. Varma − *Institute for Nanomaterials, Advanced Technologies and Innovation (CxI), Technical University of Liberec (TUL), Liberec 1 461 17, Czech Republic;* orcid.org/0000-0001-9731-6228

Complete contact information is available at: https://pubs.acs.org/10.1021/acsbiomaterials.3c01361

Author Contributions

The manuscript was written through the contributions of all authors. All authors have given approval to the final version of the manuscript.

Notes

The authors declare no competing financial interest.

Biographies

Moein Safarkhani earned his Ph.D. in December 2022 and is currently pursuing his research as a postdoctoral research assistant in South Korea. He adeptly integrates diverse fields such as molecular biology, bioengineering, and cellular biochemistry to enhance medical approaches. His primary focus lies within the realm of bioinorganic chemistry, where he pioneers innovative methods for utilizing inorganic nanocarriers to codeliver therapeutic agents and genetic material. This holds promising implications for refining medical interventions. Moreover, his contributions extend to materials synthesis, where he is trying to develop groundbreaking techniques for producing porous (in)organic nanomaterials. These methods not only streamline synthesis processes in terms of time and temperature but also align with eco-friendly and sustainable principles. With his multidimensional contributions, he stands as a dynamic force in shaping scientific progress and its application for the betterment of healthcare and sustainable practices.

Yun Suk Huh received his Ph.D. degree from the Department of Chemical and Biomolecular Engineering at KAIST in the Republic of Korea. Now he is a full Professor in the Department of Biological Engineering at Inha University, Incheon, Republic of Korea. His current research interests are to develop optical and electrochemical sensors for the highly sensitive detection of biomolecules and diseases. In addition, he is working on the synthesis of bifunctional materials for drug delivery and therapy. He has published more than 380 research articles in SCI journals.

Navid Rabiee, Ph.D., is working in several fields with a multidisciplinary approach by blending modern molecular and cellular biology/biochemical sciences with engineering principles to design the next generation of medical systems and devices for patient treatment. He is a pioneer in the field of Bioinorganic Chemistry with an emphasis on CRISPR delivery with the assistance of inorganic nanovectors. Also, he is the pioneer in developing high-gravity synthesis methods for porous (in)organic nanomaterials to reduce the synthesis temperature and time and follow green chemistry principles, which led to the foundation of a new field called "Green Biomaterials". His work has resulted in the publication of several peer-reviewed journal articles in prestigious journals, including *Nature*, *Nature Medicine*, *Nature Communications*, *The Lancet*, *Nano Today*, *ACS Applied Materials & Interfaces*, *Biomaterials*, *Advanced Materials*, *Advanced Functional Materials*, *Advanced Healthcare Materials*, etc., books, and chapters.

■ ACKNOWLEDGMENTS

This work was supported by the Korea Environment Industry & Technology Institute (KEITI) through a project to develop the Aquatic Ecosystem Conservation Research Program, funded by the Korea Ministry of Environment (MOE) (2022003040004).

■ ABBREVIATIONS

MAX, M: transition metal, A: group 11−16 A-element, X: carbon or nitrogen; MXene, "ene": highlights 2D nature akin to grapheme; MEMS, microelectromechanical systems; μPAD, microfluidic paper-based analytical device; TMD, transition metal dichalcogenides; Eb, energetic barrier; Δ*E*, reaction step energy; CVD, chemical vapor deposition; DFT, density functional theory; 2D, two-dimensional; OER, oxygen evolution reaction; HER, hydrogen evolution reaction; IoT, Internet of Things; LBG, laser-burned graphene; PDMS, polydimethylsiloxane; PI, polyamide; MWCNT, multiwalled carbon nanotubes; NFC, near field communication; ADC, analog-to-digital converter; RE, reference electrode; WE, working electrode; SVSS, standing voltage source; ECG, electrocardiogram; Aβ*O*, Amyloid *β* protein oligomer; AD, Alzheimer's disease; UA, uric acid; MF, MXene framework; MHMF, microchamber-hosted MF; e-nose, electronic nose; VOC, volatile organic compound; POCT, point-of-care testing; PDZn, Zn^{2+}-anchored polydopamine; LIGIE, laser-induced graphene interdigital electrode; DCD, diabetic comorbid depression; LI, liver impairment; ML, machine learning; SERS, surface-enhanced Raman spectroscopy; FSC, fiber-shaped supercapacitor; MFF, MXene-based fiber fabric; GQD, graphene quantum dot; PANI, polyaniline; ZIF-67, zeolitic imidazolate framework-67; CLS, complementary ligand switching

■ REFERENCES

(1) Khorsandi, D. Development of Microfluidic Platforms: Human Uterine Cervix-on-a-Chip. *Materials Chemistry Horizons* **2023**, *2* (1), 1−9.

(2) Whitesides, G. M. The origins and the future of microfluidics. *nature* **2006**, *442* (7101), 368−373.

(3) Dittrich, P. S.; Manz, A. Lab-on-a-chip: microfluidics in drug discovery. *Nat. Rev. Drug Discovery* **2006**, *5* (3), 210−218.

(4) Haeberle, S.; Zengerle, R. Microfluidic platforms for lab-on-a-chip applications. *Lab Chip* **2007**, *7* (9), 1094−1110.

(5) Khorsandi, D.; Nodehi, M.; Waqar, T.; Shabani, M.; Kamare, B.; Zare, E. N.; Ersoy, S.; Annabestani, M.; Çelebi, M. F.; Kafadenk, A. Manufacturing of microfluidic sensors utilizing 3d printing technologies: A production system. *J. Nanomater.* **2021**, *2021*, 1−16.

(6) Dabbagh Moghaddam, F.; Romana Bertani, F. Application of microfluidic platforms in cancer therapy. *Materials Chemistry Horizons* **2022**, *1* (1), 69−88.

(7) Arshavsky-Graham, S.; Segal, E. Lab-on-a-chip devices for point-of-care medical diagnostics. *Microfluidics in Biotechnology* **2020**, *179*, 247−265.

(8) Zhuang, J.; Yin, J.; Lv, S.; Wang, B.; Mu, Y. Advanced "lab-on-a-chip" to detect viruses-Current challenges and future perspectives. *Biosens. Bioelectron.* **2020**, *163*, 112291.

(9) Mahmud, M. P.; Bazaz, S. R.; Dabiri, S.; Mehrizi, A. A.; Asadnia, M.; Warkiani, M. E.; Wang, Z. L. Advances in mems and microfluidics-based energy harvesting technologies. *Advanced Materials Technologies* **2022**, *7* (7), 2101347.

(10) Pagliano, S.; Marschner, D. E.; Maillard, D.; Ehrmann, N.; Stemme, G.; Braun, S.; Villanueva, L. G.; Niklaus, F. Micro 3D printing of a functional MEMS accelerometer. *Microsystems & Nanoengineering* **2022**, *8* (1), 105.

(11) Nadar, S. S.; Patil, P. D.; Tiwari, M. S.; Ahirrao, D. J. Enzyme embedded microfluidic paper-based analytic device (μPAD): A comprehensive review. *Critical Reviews in Biotechnology* **2021**, *41* (7), 1046−1080.

(12) Noviana, E.; Ozer, T.; Carrell, C. S.; Link, J. S.; McMahon, C.; Jang, I.; Henry, C. S. Microfluidic paper-based analytical devices: from design to applications. *Chem. Rev.* **2021**, *121* (19), 11835−11885.

(13) Shi, H.; Cao, Y.; Xie, Z.; Zhao, Y.; Zhang, C.; Chen, Z. Multi-parameter photoelectric data fitting for microfluidic sweat colorimetric analysis. *Sens. Actuators, B* **2022**, *372*, 132644.

(14) Kim, S.; Lee, J.-H. Current advances in paper-based biosensor technologies for rapid COVID-19 diagnosis. *Biochip journal* **2022**, *16* (4), 376−396.

(15) Kumar, A.; Parihar, A.; Panda, U.; Parihar, D. S. Microfluidics-based point-of-care testing (POCT) devices in dealing with waves of COVID-19 pandemic: The emerging solution. *ACS applied bio materials* **2022**, *5* (5), 2046−2068.

(16) Toudeshkchoui, M. G.; Rabiee, N.; Rabiee, M.; Bagherzadeh, M.; Tahriri, M.; Tayebi, L.; Hamblin, M. R. Microfluidic devices with gold thin film channels for chemical and biomedical applications: a review. *Biomed. Microdevices* **2019**, *21*, 1−17.

(17) Rabiee, N.; Ahmadi, S.; Soufi, G. J.; Hekmatnia, A.; Khatami, M.; Fatahi, Y.; Iravani, S.; Varma, R. S. Quantum dots against Sars-cov-2: diagnostic and therapeutic potentials. *J. Chem. Technol. Biotechnol.* **2022**, *97* (7), 1640−1654.

(18) Naghdi, M.; Ghovvati, M.; Rabiee, N.; Ahmadi, S.; Abbariki, N.; Sojdeh, S.; Ojaghi, A.; Bagherzadeh, M.; Akhavan, O.; Sharifi, E.; et al. Magnetic nanostructures in nanomedicine revolution: A review of growing magnetic nanocomposites in biomedical applications. *Adv. Colloid Interface Sci.* **2022**, *308*, 102771.

(19) Jouyandeh, M.; Sajadi, S. M.; Seidi, F.; Habibzadeh, S.; Munir, M. T.; Abida, O.; Ahmadi, S.; Kowalkowska-Zedler, D.; Rabiee, N.; Rabiee, M.; et al. Metal nanoparticles-assisted early diagnosis of diseases. *OpenNano* **2022**, *8*, 100104.

(20) Nasseri, B.; Alizadeh, E.; Bani, F.; Davaran, S.; Akbarzadeh, A.; Rabiee, N.; Bahadori, A.; Ziaei, M.; Bagherzadeh, M.; Saeb, M. R. Nanomaterials for photothermal and photodynamic cancer therapy. *Applied Physics Reviews* **2022**, *9* (1), 011317.

(21) Rabiee, N.; Ahmadi, S.; Fatahi, Y.; Rabiee, M.; Bagherzadeh, M.; Dinarvand, R.; Bagheri, B.; Zarrintaj, P.; Saeb, M. R.; Webster, T. J. Nanotechnology-assisted microfluidic systems: From bench to bedside. *Nanomedicine* **2021**, *16* (3), 237−258.

(22) Ahmadi, S.; Ebrahimi Warkiani, M.; Rabiee, M.; Iravani, S.; Rabiee, N. Carbon-based nanomaterials against SARS-CoV-2: Therapeutic and diagnostic applications. *OpenNano* **2023**, *10*, 100121.

(23) Rabiee, N.; Ahmadi, S.; Iravani, S.; Varma, R. S. Functionalized silver and gold nanomaterials with diagnostic and therapeutic applications. *Pharmaceutics* **2022**, *14* (10), 2182.

(24) Rabiee, N.; Ahmadi, S.; Akhavan, O.; Luque, R. Silver and gold nanoparticles for antimicrobial purposes against multi-drug resistance bacteria. *Materials* **2022**, *15* (5), 1799.

(25) Nasseri, B.; Soleimani, N.; Rabiee, N.; Kalbasi, A.; Karimi, M.; Hamblin, M. R. Point-of-care microfluidic devices for pathogen detection. *Biosens. Bioelectron.* **2018**, *117*, 112−128.

(26) Toudeshkchouei, M. G.; Tavakoli, A.; Mohammadghasemi, H.; Karimi, A.; Ai, J.; Rabiee, M.; Rabiee, N. Recent approaches to mRNA vaccine delivery by lipid-based vectors prepared by continuous-flow microfluidic devices. *Future Medicinal Chemistry* **2022**, *14* (21), 1561−1581.

(27) Rahimnejad, M.; Rasouli, F.; Jahangiri, S.; Ahmadi, S.; Rabiee, N.; Ramezani Farani, M.; Akhavan, O.; Asadnia, M.; Fatahi, Y.; Hong, S.; et al. Engineered biomimetic membranes for organ-on-a-chip. *ACS Biomaterials Science & Engineering* **2022**, *8* (12), 5038−5059.

(28) Zhang, J.; Yan, S.; Yuan, D.; Alici, G.; Nguyen, N.-T.; Ebrahimi Warkiani, M.; Li, W. Fundamentals and applications of inertial microfluidics: A review. *Lab Chip* **2016**, *16* (1), 10−34.

(29) Tay, A.; Pavesi, A.; Yazdi, S. R.; Lim, C. T.; Warkiani, M. E. Advances in microfluidics in combating infectious diseases. *Biotechnology advances* **2016**, *34* (4), 404−421.

(30) Chaudhuri, P. K.; Ebrahimi Warkiani, M.; Jing, T.; Kenry, K.; Lim, C. T. Microfluidics for research and applications in oncology. *Analyst* **2016**, *141* (2), 504−524.

(31) Tian, F.; Cai, L.; Liu, C.; Sun, J. Microfluidic technologies for nanoparticle formation. *Lab Chip* **2022**, *22* (3), 512−529.

https://doi.org/10.1021/acsbiomaterials.3c01361
ACS Biomater. Sci. Eng. 2024, 10, 657−676

(32) Therriault, D.; White, S. R.; Lewis, J. A. Chaotic mixing in three-dimensional microvascular networks fabricated by direct-write assembly. *Nature materials* **2003**, *2* (4), 265−271.
(33) Ramezani Farani, M.; Nourmohammadi Khiarak, B.; Tao, R.; Wang, Z.; Ahmadi, S.; Hassanpour, M.; Rabiee, M.; Saeb, M. R.; Lima, E. C.; Rabiee, N. 2D MXene nanocomposites: electrochemical and biomedical applications. *Environmental Science: Nano* **2022**, *9*, 4038.
(34) Zarepour, A.; Ahmadi, S.; Rabiee, N.; Zarrabi, A.; Iravani, S. Self-Healing MXene-and Graphene-Based Composites: Properties and Applications. *Nano-micro letters* **2023**, *15* (1), 100.
(35) Novoselov, K.; Mishchenko, A.; Carvalho, A.; Castro Neto, A. 2D materials and van der Waals heterostructures. *Science* **2016**, *353* (6298), aac9439.
(36) Shuck, C. E.; Sarycheva, A.; Anayee, M.; Levitt, A.; Zhu, Y.; Uzun, S.; Balitskiy, V.; Zahorodna, V.; Gogotsi, O.; Gogotsi, Y. Scalable synthesis of Ti3C2Tx mxene. *Adv. Eng. Mater.* **2020**, *22* (3), 1901241.
(37) Gogotsi, Y.; Anasori, B. The Rise of MXenes. *ACS Nano* **2019**, *13* (8), 8491−8494.
(38) Maleki, A.; Ghomi, M.; Nikfarjam, N.; Akbari, M.; Sharifi, E.; Shahbazi, M. A.; Kermanian, M.; Seyedhamzeh, M.; Nazarzadeh Zare, E.; Mehrali, M.; et al. Biomedical applications of MXene-integrated composites: regenerative medicine, infection therapy, cancer treatment, and biosensing. *Adv. Funct. Mater.* **2022**, *32* (34), 2203430.
(39) Kim, S. J.; Koh, H.-J.; Ren, C. E.; Kwon, O.; Maleski, K.; Cho, S.-Y.; Anasori, B.; Kim, C.-K.; Choi, Y.-K.; Kim, J.; et al. Metallic Ti3C2T x MXene gas sensors with ultrahigh signal-to-noise ratio. *ACS Nano* **2018**, *12* (2), 986−993.
(40) Li, L.; Fu, X.; Chen, S.; Uzun, S.; Levitt, A. S.; Shuck, C. E.; Han, W.; Gogotsi, Y. Hydrophobic and stable MXene-polymer pressure sensors for wearable electronics. *ACS Appl. Mater. Interfaces* **2020**, *12* (13), 15362−15369.
(41) Li, X.; Huang, Z.; Shuck, C. E.; Liang, G.; Gogotsi, Y.; Zhi, C. MXene chemistry, electrochemistry and energy storage applications. *Nature Reviews Chemistry* **2022**, *6* (6), 389−404.
(42) Iravani, S.; Varma, R. S. MXene-based wearable supercapacitors and their transformative impact on healthcare. *Materials Advances* **2023**, *4*, 4317.
(43) Tavakolizadeh, M.; Atarod, M.; Seyyed Tabaei, S. J.; Sojdeh, S.; Nazarzadeh Zare, E.; Rabiee, M.; Rabiee, N. Green modified-UiO-66/MXene sandwich composites for gene-chemotherapy synergistic cancer suppression: Co-delivery of doxorubicin and pCRISPR. *Alexandria Engineering Journal* **2023**, *80*, 144−154.
(44) Deysher, G.; Shuck, C. E.; Hantanasirisakul, K.; Frey, N. C.; Foucher, A. C.; Maleski, K.; Sarycheva, A.; Shenoy, V. B.; Stach, E. A.; Anasori, B.; Gogotsi, Y. Synthesis of Mo4VAlC4MAX phase and two-dimensional Mo4VC4MXene with five atomic layers of transition metals. *ACS Nano* **2020**, *14* (1), 204−217.
(45) VahidMohammadi, A.; Rosen, J.; Gogotsi, Y. The world of two-dimensional carbides and nitrides (MXenes). *Science* **2021**, *372* (6547), No. eabf1581.
(46) Naguib, M.; Barsoum, M. W.; Gogotsi, Y. Ten years of progress in the synthesis and development of MXenes. *Adv. Mater.* **2021**, *33* (39), 2103393.
(47) Naguib, M.; Mochalin, V. N.; Barsoum, M. W.; Gogotsi, Y. 25th anniversary article: MXenes: a new family of two-dimensional materials. *Advanced materials* **2014**, *26* (7), 992−1005.
(48) Rabiee, N.; Iravani, S. MXenes and their composites: a versatile platform for biomedical applications. *Materials Chemistry Horizons* **2023**, *2* (3), 171−184.
(49) Zhang, Z.; Karimi-Maleh, H.; Wen, Y.; Darabi, R.; Wu, T.; Alostani, P.; Ghalkhani, M. Nanohybrid of antimonene@ Ti3C2Tx-based electrochemical aptasensor for lead detection. *Environmental Research* **2023**, *233*, 116355.
(50) Hantanasirisakul, K.; Gogotsi, Y. Electronic and optical properties of 2D transition metal carbides and nitrides (MXenes). *Adv. Mater.* **2018**, *30* (52), 1804779.
(51) Gogotsi, Y. Monolithic integrated MXene supercapacitors may power future electronics. *National Science Review* **2023**, *10* (3), nwad020.
(52) Hatter, C. B.; Shah, J.; Anasori, B.; Gogotsi, Y. Micro-mechanical response of two-dimensional transition metal carbonitride (MXene) reinforced epoxy composites. *Composites Part B: Engineering* **2020**, *182*, 107603.
(53) Zhang, Z.; Karimi-Maleh, H. Label-free electrochemical aptasensor based on gold nanoparticles/titanium carbide MXene for lead detection with its reduction peak as index signal. *Advanced Composites and Hybrid Materials* **2023**, *6* (2), 68.
(54) Nah, J. S.; Barman, S. C.; Zahed, M. A.; Sharifuzzaman, M.; Yoon, H.; Park, C.; Yoon, S.; Zhang, S.; Park, J. Y. A wearable microfluidics-integrated impedimetric immunosensor based on Ti3C2Tx MXene incorporated laser-burned graphene for noninvasive sweat cortisol detection. *Sens. Actuators, B* **2021**, *329*, 129206.
(55) Liu, B.; Ran, B.; Chen, C.; Shi, L.; Jin, J.; Zhu, Y. High-throughput microfluidic production of bimetallic nanoparticles on mxene nanosheets and application in hydrogen peroxide detection. *ACS Appl. Mater. Interfaces* **2022**, *14* (50), 56298−56309.
(56) Gouveia, J. D.; Viñes, F.; Illas, F.; Gomes, J. R. MXenes atomic layer stacking phase transitions and their chemical activity consequences. *Physical Review Materials* **2020**, *4* (5), 054003.
(57) Bhat, A.; Anwer, S.; Bhat, K. S.; Mohideen, M. I. H.; Liao, K.; Qurashi, A. Prospects challenges and stability of 2D MXenes for clean energy conversion and storage applications. *npj 2D Materials and Applications* **2021**, *5* (1), 61.
(58) Khan, K.; Tareen, A. K.; Iqbal, M.; Hussain, I.; Mahmood, A.; Khan, U.; Khan, M. F.; Zhang, H.; Xie, Z. Recent advances in MXenes: A future of nanotechnologies. *Journal of Materials Chemistry A* **2023**, *11*, 19764.
(59) Cao, J.; Li, T.; Gao, H.; Lin, Y.; Wang, X.; Wang, H.; Palacios, T.; Ling, X. Realization of 2D crystalline metal nitrides via selective atomic substitution. *Science advances* **2020**, *6* (2), No. eaax8784.
(60) Liu, J.; Zhou, F.; Wang, S.; Zeng, R., Novel Nitride-Based Electrodes for Solid-State Batteries. In *Solid State Batteries Vol. 2: Materials and Advanced Devices*; American Chemical Society: 2022; pp 15−38.
(61) Lee, C.-S.; Wang, M.; Clyde, P. M.; Mao, X.; Brownawell, B. J.; Venkatesan, A. K. 1, 4-Dioxane removal in nitrifying sand filters treating domestic wastewater: Influence of water matrix and microbial inhibitors. *Chemosphere* **2023**, *324*, 138304.
(62) Yin, Y.; Gong, Q.; Yi, M.; Guo, W. Emerging Versatile Two-Dimensional MoSi2N4 Family. *Adv. Funct. Mater.* **2023**, *33* (26), 2214050.
(63) Khazaei, M.; Wang, J.; Estili, M.; Ranjbar, A.; Suehara, S.; Arai, M.; Esfarjani, K.; Yunoki, S. Novel MAB phases and insights into their exfoliation into 2D MBenes. *Nanoscale* **2019**, *11* (23), 11305−11314.
(64) Zhang, B.; Zhou, J.; Sun, Z. MBenes: progress, challenges and future. *Journal of Materials Chemistry A* **2022**, *10*, 15865.
(65) Chen, Y.; Qin, H.; Zhou, J.; Yang, T.; Sun, B.; Ni, Y.; Wang, H.; Redfern, S. A. T.; Miao, M.; Lin, H.-Q.; Feng, Y. P. Unveiling Interstitial Anionic Electron-Driven Ultrahigh K-Ion Storage Capacity in a Novel Two-Dimensional Electride Exemplified by Sc3Si2. *J. Phys. Chem. Lett.* **2022**, *13* (32), 7439−7447.
(66) Li, Y.; Li, J.; Wan, L.; Li, J.; Qu, H.; Ding, C.; Li, M.; Yu, D.; Fan, K.; Yao, H. The First-Principle Study on Tuning Optical Properties of MA2Z4 by Cr Replacement of Mo Atoms in MoSi2N4. *Nanomaterials* **2022**, *12* (16), 2822.
(67) Sun, X.; Zheng, J.; Yao, Z.; Deng, S.; Pan, Z.; Wang, S.; Wang, J. DFT investigation of single metal atom-doped 2D MA2Z4 materials for NO electrocatalytic reduction to NH3. *J. Phys. Chem. C* **2022**, *126* (41), 17598−17607.
(68) Chen, Y.; Tian, S.; Tang, Q. First-principles studies on electrocatalytic activity of novel two-dimensional MA2Z4 monolayers toward oxygen reduction reaction. *J. Phys. Chem. C* **2021**, *125* (41), 22581−22590.
(69) Wang, X.; Ju, W.; Wang, D.; Li, X.; Wan, J. Flexible MA2Z4 (M= Mo, W; A= Si, Ge and Z= N, P, As) monolayers with

outstanding mechanical, dynamical, piezoelectric properties and anomalous dynamic polarization. *Phys. Chem. Chem. Phys.* **2023**, *25*, 18247.
(70) Sharma, A.; Rangra, V.; Thakur, A. Synthesis, properties, and applications of MBenes (two-dimensional metal borides) as emerging 2D materials: a review. *J. Mater. Sci.* **2022**, *57* (27), 12738−12751.
(71) Ozdemir, I.; Kadioglu, Y.; Yüksel, Y.; Akıncı, D. C.; Aktürk, O. Ü.; Aktürk, E.; Ciraci, S. Columnar antiferromagnetic order of a MBene monolayer. *Phys. Rev. B* **2021**, *103* (14), 144424.
(72) Zhou, S.; Yang, X.; Pei, W.; Jiang, Z.; Zhao, J. MXene and MBene as efficient catalysts for energy conversion: roles of surface, edge and interface. *Journal of Physics: Energy* **2021**, *3* (1), 012002.
(73) Xu, T.; Wang, Y.; Xiong, Z.; Wang, Y.; Zhou, Y.; Li, X. A rising 2D star: novel MBenes with excellent performance in energy conversion and storage. *Nano-Micro Letters* **2023**, *15* (1), 6.
(74) Zhang, S.; Zahed, M. A.; Sharifuzzaman, M.; Yoon, S.; Hui, X.; Chandra Barman, S.; Sharma, S.; Yoon, H. S.; Park, C.; Park, J. Y. A wearable battery-free wireless and skin-interfaced microfluidics integrated electrochemical sensing patch for on-site biomarkers monitoring in human perspiration. *Biosens. Bioelectron.* **2021**, *175*, 112844.
(75) Li, Q.-F.; Chen, X.; Wang, H.; Liu, M.; Peng, H.-L. Pt/MXene-based flexible wearable non-enzymatic electrochemical sensor for continuous glucose detection in sweat. *ACS Appl. Mater. Interfaces* **2023**, *15* (10), 13290−13298.
(76) Zahed, M. A.; Kim, D. K.; Jeong, S. H.; Selim Reza, M.; Sharifuzzaman, M.; Pradhan, G. B.; Song, H.; Asaduzzaman, M.; Park, J. Y. Microfluidic-Integrated Multimodal Wearable Hybrid Patch for Wireless and Continuous Physiological Monitoring. *ACS Sensors* **2023**, *8*, 2960.
(77) Wen, X.-H.; Zhao, X.-F.; Wang, X.-H.; Wang, Y.; Guo, J.-C.; Zhou, H.-G.; Zuo, C.-T.; Lu, H.-L. Fe3O4/MXene Nanosphere-Based Microfluidic Chip for the Accurate Diagnosis of Alzheimer's Disease. *ACS Applied Nano Materials* **2022**, *5* (10), 15925−15933.
(78) Zhao, P.; Liu, Y.; Chen, Y.; Yang, M.; Zhao, S.; Qi, N.; Wang, Y.; Huo, D.; Hou, C. Hemin-Functionalized Microfluidic Chip with Dual-Electric Signal Outputs for Accurate Determination of Uric Acid. *ACS Appl. Mater. Interfaces* **2022**, *14* (36), 41369−41378.
(79) Ding, X.; Zhang, Y.; Zhang, Y.; Ding, X.; Zhang, H.; Cao, T.; Qu, Z.-b.; Ren, J.; Li, L.; Guo, Z.; et al. Modular Assembly of MXene Frameworks for Noninvasive Disease Diagnosis via Urinary Volatiles. *ACS Nano* **2022**, *16* (10), 17376−17388.
(80) Yang, K.; Zhang, C.; Zhu, K.; Qian, Z.; Yang, Z.; Wu, L.; Zong, S.; Cui, Y.; Wang, Z. A Programmable plasmonic gas microsystem for detecting arbitrarily combinated volatile organic compounds (VOCs) with ultrahigh resolution. *ACS Nano* **2022**, *16* (11), 19335−19345.
(81) Zhu, X.; Zhang, Y.; Man, Z.; Lu, W.; Chen, W.; Xu, J.; Bao, N.; Chen, W.; Wu, G. Microfluidic-Assembled Covalent Organic Frameworks@ Ti3C2Tx MXene Vertical Fibers for High-Performance Electrochemical Supercapacitors. *Adv. Mater.* **2023**, *35*, 2307186.
(82) Qiu, H.; Qu, X.; Zhang, Y.; Chen, S.; Shen, Y. Robust PANI@ MXene/GQDs Based Fibre Fabric Electrodes via Microfluidic Wet-Fusing Spinning Chemistry. *Adv. Mater.* **2023**, *35*, 2302326.
(83) Wu, G.; Sun, S.; Zhu, X.; Ma, Z.; Zhang, Y.; Bao, N. Microfluidic Fabrication of Hierarchical-Ordered ZIF-L (Zn)@ Ti3C2Tx Core-Sheath Fibers for High-Performance Asymmetric Supercapacitors. *Angew. Chem.* **2022**, *134* (8), No. e202115559.
(84) Zhang, Y.; Zhu, X.; Sun, S.; Guo, Q.; Xu, M.; Wu, G. Ordered Interface Engineering Enabled High-Performance Ti3C2T x MXene Fiber-Based Supercapacitors. *Energy Fuels* **2022**, *36* (14), 7898−7907.
(85) Yang, K.; Zhu, K.; Wang, Y.; Qian, Z.; Zhang, Y.; Yang, Z.; Wang, Z.; Wu, L.; Zong, S.; Cui, Y. Ti3C2T x MXene-Loaded 3D Substrate toward On-Chip Multi-Gas Sensing with Surface-Enhanced Raman Spectroscopy (SERS) Barcode Readout. *ACS Nano* **2021**, *15* (8), 12996−13006.
(86) Rabiee, N.; Dokmeci, M. R.; Zarrabi, A.; Makvandi, P.; Saeb, M. R.; Karimi-Maleh, H.; Jafarzadeh, S.; Karaman, C.; Yamauchi, Y.; Warkiani, M. E.; et al. Green Biomaterials: fundamental principles. *Green Biomaterials* **2023**, *1*, 1−4.

https://doi.org/10.1021/acsbiomaterials.3c01361
ACS Biomater. Sci. Eng. 2024, 10, 657−676